Inference of cell type-specific gene regulatory networks on cell lineages from single cell omic datasets

Shilu Zhang[1], Saptarshi Pyne[1], Stefan Pietrzak[1], Alireza Fotuhi Siahpirani[1], Rupa Sridharan[1,3], and Sushmita Roy[1,2*]

[1]Wisconsin Institute for Discovery, University of Wisconsin-Madison, Madison, WI, USA

[2]Department of Biostatistics and Medical Informatics, University of Wisconsin-Madison, Madison, WI, USA

[3]Department of Cell and Regenerative Biology, University of Wisconsin-Madison, Madison, WI, USA

[*]To whom correspondence should be addressed. Corresponding author email: sroy@biostat.wisc.edu

Abstract

Cell type-specific gene expression patterns are outputs of transcriptional gene regulatory networks (GRNs) that connect transcription factors and signaling proteins to target genes. These networks reconfigure during dynamic processes such as cell fate specification to drive diverse cellular states. Single-cell transcriptomic technologies, such as single cell RNA-sequencing (scRNA-seq) and single cell Assay for Transposase-Accessible Chromatin using sequencing (scATAC-seq), can examine the transcriptional state of individual cells, allowing the study of cell-type specific gene regulation at unprecedented detail. However, current approaches to infer cell type-specific gene regulatory networks from these datasets are limited in their ability to integrate scRNA-seq and scATAC-seq measurements and to model network dynamics on a cell lineage. To address this challenge, we have developed single-cell Multi-Task Network Inference (scMTNI), a multi-task learning framework to infer the gene regulatory network for each cell type on a lineage from scRNA-seq and scATAC-seq data. Using simulated, published and newly collected single cell omic datasets, we show that scMTNI is able to accurately infer gene regulatory networks and captures meaningful network dynamics that identify GRN components associated with cell type transitions. Application of our method to mouse cellular reprogramming identified key regulators associated with cell populations that reprogram versus those that are stalled. Taken together, scMTNI is a powerful framework to infer cell type-specific gene regulatory networks and their dynamics from scRNA-seq and scATAC-seq datasets.

Introduction

Transcriptional gene regulatory networks (GRNs) specify connections between regulatory proteins and target genes and determine the spatial and temporal expression patterns of genes[1,2]. These networks reconfigure during dynamic processes such as development or disease progression, to specify cell type specific expression levels. Recent advances in single cell omic techniques such as single cell RNA-sequencing (scRNA-seq) and single cell Assay for Transposase-Accessible Chromatin using sequencing (scATAC-seq)[3] enable collecting high resolution molecular phenotypes of a developing system and offer unprecedented opportunities for the discovery of cell type-specific regulatory networks and their dynamics. However, computational methods to systematically leverage these datasets to identify regulatory networks driving cell type-specific expression patterns, are limited.

Existing methods of network inference from single cell omic data[4–16] have primarily used transcriptomic measurements and have low recovery of experimentally verified interactions[17,18]. Recently a small number of methods have attempted to integrate scRNA-seq and scATAC-seq datasets[19,20] to examine gene regulation, however, the primary focus of these methods is to define cell clusters and the network is defined entirely based on accessible sequence-specific motif matches. This restricts the class of regulators that can be incorporated into the regulatory network to those with known motifs. Furthermore, existing methods infer a single GRN for the entire dataset or do not model the cell population structure which is important to discern dynamics and transitions in the inferred networks for cell type-specificity.

To overcome the limitations of existing methods, we have developed single-cell Multi-Task Network Inference (scMTNI), a multi-task learning framework that integrates the cell lineage structure, scRNA-seq and scATAC-seq measurements to enable joint inference of cell type-specific GRNs. scMTNI takes as input a cell lineage tree, scRNA-seq data and scATAC-seq based prior networks for each cell type. scMTNI uses a novel probabilistic prior to incorporate the lineage structure during network inference and outputs GRNs for each cell type on a cell lineage. We performed a comprehensive benchmarking study of multi-task learning approaches including scMTNI on simulated data and show that incorporation of multi-task learning and tree structure is beneficial for GRN inference.

We applied scMTNI to a novel scRNA-seq and scATAC-seq time course dataset for cellular reprogramming in mouse and a published scRNA-seq and scATAC-seq cell-type specific dataset for human hematopoietic differentiation. We demonstrate the advantage of integration of scATAC-seq and scRNA-seq datasets for inferring cell type specific GRNs and their dynamics. We examined how the inferred networks change along the trajectory and identified regulators and network components specific to dif-

ferent parts of the lineage tree. Our predictions include known as well as novel regulators of cell populations transitioning to different lineage paths, providing insight into regulatory mechanisms associated with hematopoietic specification and reprogramming efficiency.

Results

Single-cell Multi-Task learning Network Inference (scMTNI) for defining regulatory networks on cell lineages

We developed scMTNI, a multi-task graph learning framework for inferring cell type-specific gene regulatory networks from scRNA-seq and scATAC-seq datasets (**Figure 1A**), where a cell type is defined by a cluster of cells with a distinct transcriptional and accessibility profile. scMTNI models a GRN as a Dependency network[21], a probabilistic graphical model with random variables representing genes and regulators, such as transcription factors (TFs) and signaling proteins. scMTNI takes as input cell clusters with gene expression and accessibility profiles and a lineage structure linking the cell clusters (**Figure 1**). Such inputs can be obtained from existing methods for integrative clustering[22] and lineage construction[23]. scMTNI uses the scATAC-seq data for each cell cluster to define cell type-specific sequence motif-based TF-target interactions (e.g., a motif for a particular TF, which is accessible only in specific cell types will result in a TF-target interaction only in those cell types) which are used as a prior to guide network inference (**Methods**). The output of scMTNI is a set of cell type-specific GRNs one for each cell cluster in the lineage tree. scMTNI's multi-task learning framework incorporates a novel lineage tree prior, which uses the lineage tree structure to influence the similarity of gene regulatory networks on the lineage. This prior models the change of a GRN from a start state (e.g., progenitor cell state) to an end state (e.g. more differentiated state) as a series of individual edge-level probabilistic transitions. While scMTNI was developed to incorporate both scRNA-seq and scATAC-seq data, it can be applied to situations where scATAC-seq, and therefore a cell type-specific prior network, is not available. We refer to the versions of our approach as scMTNI+prior and scMTNI depending upon whether it uses prior knowledge or not. The output networks of scMTNI are analyzed using two dynamic network analysis methods: edge-based k-means clustering and topic models (**Figure 1B**). These approaches identify key regulators and subnetworks associated with a particular cell cluster or a set of cell clusters on a branch.

Multi-task learning algorithms outperform single-task algorithms for single cell network inference

To evaluate scMTNI and other existing algorithms with known ground truth networks on single-cell transcriptomic data, we set up a simulation framework, which entailed creation of a cell lineage, generating

synthetic networks and corresponding single-cell expression datasets for each cell type on the lineage (**Figure 2A**). We used a probabilistic process of network structure evolution to simulate the network structure for three cell types, each containing 15 regulators and 65 genes and between 202-239 edges (**Methods**). Next, we applied BoolODE[17] to simulate the *in silico* single-cell expression data using each cell type's simulated network. To mimic the sparsity in single-cell expression data, we set 80% of the values to 0. We created three datasets with different numbers of cells: 2000, 1000, 200, referred here as dataset 1, dataset 2, dataset 3.

We asked whether multi-task learning is beneficial compared to single-task learning for network inference from scRNA-seq data. To this end we compared scMTNI and four other multi-task learning algorithms, MRTLE[24], GNAT[25], Ontogenet[26], and AMuSR[27] to three single-task algorithms, LASSO regression[28], INDEP, and SCENIC[29] (**Methods**). Of these methods only SCENIC uses a non-linear regression model while the others are based on linear models. INDEP is similar to scMTNI but does not incorporate the lineage prior. Each algorithm was applied within a stability selection framework and evaluated with Area under the Precision recall curve (AUPR) and F-score of top k edges, where k is the number of edges in the true network (**Figure 2B, C**). On dataset 1, based on AUPR, scMTNI, MRTLE and AMuSR are able to recover the network structure (**Figure 2B**) better than the other multi-task learning and single-task learning algorithms. Ontogenet performs better than the single-task learning algorithms in at least two cell types. Finally, GNAT performs comparably to the single-task learning algorithms. When comparing algorithms based on F-score of top k edges, we have similar observations that scMTNI and MRTLE have a better performance than other algorithms (**Figure 2C**). Ontogenet performs better than LASSO and INDEP in at least two cell types, and comparable to SCENIC, except that Ontogenet in cell type 3 is worse than SCENIC. GNAT is comparable to the single-task learning algorithms for at least 2 of the cell types. The low F-score of AMuSR is because the inferred networks are too sparse, with fewer than 100 edges, while the other algorithms inferred similar number of edges with the true networks. These results remain consistent for datasets 2 and 3 which have fewer cells (1000 and 200, respectively), scMTNI and MRTLE remain superior in performance than other algorithms measured by both AUPR and F-score (**Figure 2B**, **C**). We expect scMTNI to be better since the network simulation procedure is similar, but the data generated is different and independent. Finally, we aggregated the results across all three cell types and datasets to obtain an overall comparison of the algorithms. Here we considered algorithms across all parameter settings tested as well as the best parameter setting determined by the best F-score or AUPR. Based on the AUPR of "all parameter setting" , we found that multi-task learning methods, especially scMTNI and MRTLE are generally better than single-task

learning methods with higher AUPRs (**Supplementary Figure 1A**,**C**). AMuSR also outperformed the single-task algorithms based on AUPRs, although this was not as significant as MRTLE and scMTNI. When considering the "best parameter setting" the methods were not significantly different when using AUPR, though MRTLE and scMTNI had the highest AUPR (**Supplementary Figure 1B**,**D**). When using the F-score, scMTNI and MRTLE remained top performing algorithms for the "all parameter setting" (**Supplementary Figure 2A**,**C**) and the "best parameter setting" (**Supplementary Figure 2B**,**D**). Further, GNAT and Ontogenet had a higher F-score than the single-task learning method LASSO for the "all parameter" and "best parameter" settings. AMuSR suffered for the F-score metric due to the high sparsity in the inferred networks. Across different single-task algorithms, LASSO had the worst performance. Overall, the results on the simulated networks suggest that multi-task learning algorithms have a better performance than single-task algorithms for network inference on sparse datasets, similar to single-cell transcriptomic data. Furthermore, scMTNI and MRTLE are able to more accurately infer networks than other multi-task learning algorithms.

Inference of gene regulatory networks of somatic cell reprogramming to induced pluripotent stem cells

Cellular reprogramming is the process of converting cells in a differentiated state to a pluripotent state and is important in regenerative medicine as well as for generating patient-specific disease models. However, this process is inefficient as a small fraction of cells get reprogrammed to the pluripotent state[30]. To gain insight into the gene regulatory networks that govern the dynamics of this process, we profiled single cell accessibility (scATAC-seq) during the reprogramming process from mouse embryonic fibroblasts (MEFs) to the induced pluripotent state and four intermediate timepoints, day3, day6, day9 and day12, to constitute a dataset of 6 timepoints. We used LIGER to integrate the scRNA-seq and scATAC-seq datasets (**Figure 3A**, **B**) and identified 8 clusters (**Methods**). Of these clusters, C4 is MEF-specific while C5 is ESC-specific (**Figure 3C**, **D**) and showed good integration of the scRNA-seq and scATAC-seq profiles. We removed C6 as it did not have scRNA-seq cells and applied a minimum spanning tree (MST[23]) approach to construct the cell lineage tree from the 7 cell clusters with both scRNA-seq and scATAC-seq (**Methods**, **Figure 3E**). The MEF-specific cluster (C4) is at one end of the tree, while the ESC-specific cluster (C5) is at the other end. This is consistent with the starting and end state of the reprogramming process and we considered C4 to represent the root of the tree.

We applied scMTNI, scMTNI+prior (scMTNI with prior network), INDEP, INDEP+prior (INDEP with prior network) and SCENIC to this dataset (**Figure 3F**). We used the matched scATAC-seq clus-

ters to obtain transcription factor (TF)-target prior interactions for each scRNA-seq cluster needed for INDEP+prior and scMTNI+prior (**Methods**). We assessed the quality of the inferred networks by comparing to three gold standard datasets in mouse embryonic stem cells (mESCs, **Table 2**), one derived from ChIP-seq experiments (referred to as "ChIP") from ESCAPE or ENCODE databases[31,32], one from regulator perturbation experiments (referred to as "Perturb")[31,33], and the third from the intersection of edges in ChIP and Perturb (referred to as "ChIP+Perturb"). We compared the performance of the methods using F-score on the top 500, 1k and 2k edges across methods (**Figure 3F**, **Supplementary Figure 3, 4**). On Perturb and Perturb+ChIP, scMTNI+Prior had a higher average performance, outperforming other methods significantly in Perturb. On ChIP, SCENIC was generally better than other methods. To examine the poorer performance of scMTNI+Prior for the ChIP gold standard, we compared the regulators and targets in the inferred networks from each method. Between SCENIC and scMTNI, the number of regulators are similar, but SCENIC's networks have more target genes, which recovered more targets from the gold standard datasets, resulting in a higher F-score. scMTNI+prior outperformed scMTNI in all but the ChIP dataset, and INDEP+prior outperformed INDEP, indicating that addition of priors based on scATAC-seq data was beneficial.

To gain an initial assessment of the network dynamics on the cell lineage, we computed F-score between each pair of inferred networks defined by the top 4k edges (**Figure 3G**). Both scMTNI and scMTNI+prior networks diverged in a manner consistent with the lineage structure. scMTNI networks formed three groups of cell types, (C4, C8, C1, C7), (C2, C3) and (C5 (ESC)). scMNTI+prior found similar groupings but placed C5 (ESC) closer to (C1, C7, C8, C4) branch. Both methods showed that C5 is closest to C1, which could be an important transitioning state of cells during reprogramming. SCENIC showed similarity among C1, C4, C7, however had lower similarity scores for most pairwise comparisons which made it difficult to discern a clear lineage structure. The networks inferred by the other methods were very divergent which is not biologically realistic because the reprogramming system is heterogeneous with a number of transitioning populations. Overall, these results suggest that scMTNI+prior recovered regulatory networks are of high quality and the networks exhibit a gradual rewiring of structure from the MEF to the pluripotent state.

scMTNI predicts key regulatory nodes and GRN components that are rewired during reprogramming

To gain insight into which cell populations successfully reprogram versus those that do not and to further characterize these different cell clusters, we examined the specific rewired network components

in each cell type-specific network inferred by scMTNI+prior using two complementary approaches: k-means edge clustering and Latent Dirichlet Allocation (LDA, **Methods**). In the k-means edge clustering approach, we represented each edge in the top 4k confidence set of any cell cluster, by a vector of confidence scores in each cell cluster-specific network (if an edge is not inferred in the network it is assigned a weight of 0). Next, we clustered edges based on their edge confidence pattern into 20 clusters determined by the Silhouette Coefficient optimization (**Figure 4A**). The largest "edge clusters" exhibited interactions specific to one cell cluster (e.g., E4, E6, E7, E11, E13, E15 and E16), while smaller clusters exhibited conserved edges for more than one cell cluster (e.g., E2, E5, E12). To interpret these edge clusters, we identified the top regulators associated with each of the edge clusters (**Figure 4B**). E16, which was MEF-specific (C4) had Npm1, Nme2, Thy1, Ddx5 and Loxl2 as the top regulators which are known MEF-specific genes. In contrast, E11, which was ESC-specific (C5) had Klf4, Lhx2, Elf4 which have known roles in stem cell maintenance (Klf4) and differentiation into neural (Lhx2[34]) and hematopoieitic lineage (Elf4[35]). Edge clusters that shared edges across multiple cell clusters, e.g. E5 (C4, C8 and C1), shared some of the top-ranking regulators such as Npm1 and Thyb1 with the MEF-specific cluster and also identified other fibroblast-specific genes such as Col5a2 and Ybx1. Finally, E2 which comprised shared edges between cell clusters C1 and C5, contained Esrrb, as its top regulator (**Figure 4B**). Esrrb plays an important role for establishing naive pluripotency. This further supports the lineage structure that C1 likely represents a population of cells that are committed to becoming pluripotent.

While the k-means analysis identified regulatory hubs specific to individual cell clusters, it was challenging to identify sub-network components that rewired at specific branch points likely because it treats each edge independently. We developed an approach by adopting Latent Dirichlet Allocation (LDA) that was recently used to study regulatory network rewiring from transcription factor ChIP-seq datasets[36] (**Methods**). In this approach, each TF is treated as a "document" and target genes are treated as "words" in the document. Each document (TF) is assumed to have words (genes) from a mixture of topics, each topic in turn interpreted as a pathway. TFs across cell clusters are treated as separate documents. We applied LDA with $k = 10$ topics (**Figure 4C**, **D**, **Supplementary Figure 5,6, 7**), and examined each of the topics based on their Gene Ontology process enrichment (**Supplementary Figure 8**), and the tendency and identity of specific regulators to rewire across the cell clusters (**Methods**). Topic 3 networks were among the most divergent networks across the cell populations and identified several known regulators for the pluripotency fate (**Figure 4C**). In particular, Esrrb was a hub in C5 (ESC) and C1 (closest to ESC) but absent in the other cell clusters. Topic 3 is enriched for cell cycle and developmental terms (**Supplementary Figure 8**). Comparison of the regulators in the (C1,C5) branch and (C7, C3,

C2) branch showed that the latter branch had regulators such as Wt1. Wt1 was a major regulator in the starting MEF cluster as well suggesting the incomplete suppression of the MEF-specific program in the C7-C3-C2 branch. Wt1 is an important regulator of cellular developmental processes and can act both as a tumor suppressor and an oncogene[37]. Topic 9 was also interesting in that it identified the persistence of the regulators Ccng1 and Nme2 from the MEF-specific cell cluster (C4) in the C7-C3-C2 branch. Ccng1 is a cyclin that is part of the p53 pathway, which has been previously identified to be associated with the inefficiency of cellular reprogramming[38,39]. Nme2 is known to regulate Myc, which is an oncogene and also one of the four reprogramming factors[40]. The cellular reprogramming process has been considered to be similar to tumorigenesis which is supported by the identification of regulators associated with cancer signaling pathways for populations that do not reprogram. Inhibition of these regulators could potentially improve the reprogramming process. In total, using scMTNI and network rewiring analysis we identified known cell population-specific regulators and also predicted new regulators that can be perturbed to examine the impact on cellular reprogramming efficiency.

Inferring gene regulatory networks in human hematopoietic differentiation

To examine the utility of scMTNI in a different cell fate specification system, we applied scMTNI to a published scATAC-seq and scRNA-seq dataset for human hematopoietic differentiation[41]. This dataset profiled accessibility and transcriptomic state of immunophenotypic populations that were sorted based on cell surface markers in hematopoietic differentiation and enabled studies of how multipotent progenitors transit into lineage-restricted cell states. We considered the cell populations measured with both scATAC-seq and scRNA-seq datasets: hematopoietic stem cell (HSC), common myeloid progenitor (CMP), granulocyte-macrophage progenitors (GMP) and monocyte (Mono). These populations are known to be heterogeneous comprising multiple sub-populations[41]. To identify these sub-populations we again applied LIGER[22] and identified 10 integrated clusters of RNA and accessibility (**Figure 5A-D**). Most clusters exhibited a mixed composition: C8 is mainly composed of HSCs but also included CMP0 cells; C6 and C9 are composed of GMP and CMP0 cells. C1 (73 cells) and C4 (37 cells) were mainly composed of Mono cells and were combined into C1. C5 had too few RNA cells (22 cells) and was excluded from further analysis. We next inferred a cell lineage tree from these 8 cell clusters using a minimal spanning tree approach[23] as described in the reprogramming study (**Figure 5E**, **Methods**). As C8 is largely made up of HSC cells and HSC is the starting cell type, we treat C8 as the root of the lineage.

We applied the same set of network inference algorithms to this dataset as the reprogramming dataset:

scMTNI, scMTNI+prior, INDEP, INDEP+prior and SCENIC. We assessed the quality of the inferred networks from each method by comparing them to gold-standard edges from published ChIP-seq and regulator perturbation assays from several human hematopoietic cell types. This included ChIP-seq datasets from the UniBind database (Unibind[42]), ChIP-seq (Cus_ChIP) and regulator perturbation (Cus_KO) experiments in the GM12878 lymphoblastoid cell line from Cusanovich et al[43] and the intersection of ChIP and perturbation studies (Cus_KO+Cus_ChIP, Cus_KO+Unibind). In total we had five gold standard networks. We used F-score of the top 500, 1k, 2k edges in the inferred network (**Methods**, **Figure 5F**, **Supplementary Figure 9**). The relative performance of the algorithms depended upon the gold standard. Algorithms that did not use priors (INDEP, SCENIC and scMTNI) performed comparably (with no significant difference) on three of the five gold standards. On Unibind and Cus_KO+Unibind, SCENIC is significantly better than INDEP and scMTNI (**Supplementary Figure 10**). Methods that used priors, INDEP+prior, scMTNI+prior, were generally better than methods without priors. INDEP+prior and scMTNI+prior are comparable across the gold standard datasets with no significant difference in performance. For the Unibind dataset, we had ChIP-seq based gold standard edges for different blood cell types, with 1 to 48 transcription factors (**Table 3**). When comparing to these cell type-specific gold standards, prior based methods have a better performance especially for datasets with more TFs among top 500 and 1k edges (**Supplementary Figure 11,Supplementary Figure 12**). Furthermore, INDEP+prior had the best overall performance indicating that incorporation of accessibility priors is more important rather than the lineage information. However, these gold standards were much smaller and therefore can assess smaller portion of the inferred networks.

We next examined the inferred networks for the extent of change on the lineage structure (**Figure 5G**). The single-task learning methods INDEP and INDEP+prior exhibited a low overlap across each pair of cell lines and did not as such obey the lineage structure. SCENIC recovers part of the lineage structure, but placed C7 (common myeloid) close to C6 (granulocyte-macrophage progenitors (GMP)) rather than C10, which has similar sample composition as C7. In contrast, scMTNI and scMTNI+prior were able to find two groups of cell types, one corresponding to HSC and CMP2 branch consisting of C8, C3 and C2, and the second corresponding to the CMP0, CMP1 and GMP branch (C6, C9, C10 and C7). The excessive divergence identified by the single-task learning methods makes it difficult to identify and prioritize specific network level changes driving cell fate decisions.

Inferring shared and lineage-specific regulators for hematopoietic differentiation

Similar to our cellular reprogramming study, we examined the scMTNI+prior networks to identify cell type-specific regulators and network components (**Figure 6**). We applied k-means edge clustering to top 5k edges in any of the cell clusters and identified 19 edge clusters (**Methods**). Compared to the reprogramming study, a larger portion (94% vs 86%) of the edges are specific to one cell cluster (**Figure 6A**). We used these edge clusters to identify differences among cell clusters which had similar compositions of the initial cell types identified based on cell surface markers, e.g., C7 and C10 had similar composition of CMP0, CMP1, CMP2 cells and C6 and C9 had similar composition of GMP and CMP cells. Edge cluster E2 had edges specific to cell cluster C7 and was associated with PLEX, YBX1, EEF1A1, TSC22D3. PLEK and YBX1[44] are known to be involved in directing fate of HSCs, while both EEF1A1 and TSC22D3 have immune-related functions. In contrast, E8 which had edges specific to C10 had different regulators, namely KLF7, ETV5, MBD2, ZNF202, EPM2A, ULK4. Of these, KLF7, ETV5 and MBD2 have known regulatory roles in hematopoiesis, with ETV5 regulating a population of Th9 cells[45] and KLF7 suppressing the formation of myeloid cells[46]. Edge cluster E11, which was specific to C6 ranked SP4, TYR03, ZNF417, MNDA highly. MNDA is associated with granulocyte-monocyte lineage[47]. In contrast, E6, which was specific to C9 had a different set of top regulators including L3MBTL4, GABPA, ELF4, and RGS14. Both GABPA and ELF4 have important roles in hematopoiesis[48,49]. A few edge clusters represented shared network components, e.g. E19 had edges from C6, C9, C10, C7 that represented the GMP and CMP populations and E12 representing edges from C10 and C7. Both E19 and E12 had YBX1 and TSC22D3 as top regulators (**Figure 6B**). YBX1, is known to have high expression in myeloid progenitor cells[44], and regulates CCL5 expression during monocyte/macrophage differentiation[50]. TSC22D3, which is a glucocorticoid leucine zipper[51], is involved in differentiation of hematopoietic stem cells[52]. Taken together, the k-means edge clustering approach helped identify the key regulators with known or plausible roles in hematopoiesis that could explain the differences among the cell clusters.

To identify cell type-specific network rewiring that are associated with lineage decisions, we again examined the regulatory networks of each cell cluster using LDA (**Methods**, **Figure 6C**, **D**). The topics were enriched for diverse biological processes such as cell cycle (Topic 1 and 8, **Supplementary Figure 16**), blood related processes (Topic 9) and represented subnetworks with different extents of conservation across the lineage. For example, topic 2 showed a gradual rewiring of an ID2-specific network from the HSC populations (C8, C3, C2), to KLF1 and MYC centered networks for C7 and C10 which represented the CMP0 population. ID2 is known to negatively regulate differentiation, which is con-

sistent with its presence in the C8, C3, C2 branches. KLF1 is an essential regulator for the erythroid lineage[53,54] , which is derived from the myeloid progenitor cells and therefore the association of KLF1 with these cells is consistent with the literature. Topics 1, 6 and 10 exhibited a conserved core around HMGB2, TSC22D3, and YBX1 respectively, across all cells clusters (**Supplementary Figure 13, 14, 15**). HMGB2 is an important regulator for HSCs[55]. Both YBX1 and TSC22D3, which were also identified in our k-means analysis, have known role in hematopoeisis[44]. Topic 8 was associated with various cell cycle and chromatin remodeling regulators such as TOP2A, CDC20 and CCNB1 (**Supplementary Figure 15, 16**). Taken together, the LDA analysis identified differential subnetworks centered to candidate cell fate drivers in hematopoeisis that could be followed up with functional studies.

Discussion

Single-cell technologies have transformed our ability to study cellular heterogeneity and cell-type specific gene regulation of known and novel cell populations. Defining gene regulatory networks from scRNA-seq data of developmental systems has remained challenging as most existing methods have assumed a static view of the GRN and do not leverage accessibility to inform the GRN structure. To address this need, we develop single-cell Multi-Task Network Inference (scMTNI), a probabilistic graphical model-based approach that uses multi-task learning to infer cell type-specific GRNs on a cell lineage tree by integrating scRNA-seq and scATAC-seq data and model the dynamics of these regulatory interactions on a lineage.

Multi-task learning is well-suited for the inference of cell type-specific GRNs. However, a key question is how to implement multi-task learning for GRN inference. A number of multi-task learning algorithms were developed for inferring GRNs and functional networks from bulk transcriptomic data but have not been systematically compared for their effectiveness on single-cell transcriptomic data. Some approaches, such as AMuSR[27] have used a flat hierarchy where all the tasks are considered equally related. For heterogeneously related datasets, a hierarchy or a tree is well-suited to model the dependence across datasets. Such hierarchies can be implemented as a phylogenetic tree with observed data at the tips of the tree as in GNAT[25] and MRTLE[24], or as a cell-lineage tree with observations at all nodes in the tree. scMTNI and MRTLE both use a tree-based structure prior, whereas AMuSR, GNAT and Ontogenet used a regularized regression parameter to implement multi-task learning. scMTNI and MRTLE have better performance in predicting the gene regulatory relationships than single-task learning algorithms. The performance of Ontogenet is better than the single-task learning algorithms LASSO and INDEP in at least two cell types, and comparable to SCENIC. A prominent factor contributing to the difference in the performance of the algorithms was whether the models inferred a directed graph versus an undirected graph, with GNAT generally suffering likely due to this reason. Performance of GNAT is worst among multi-task learning algorithms and comparable to the single-task learning algorithms. We speculate that the undirected relationship in the graphical model of GNAT might be a reason that the performance is not as good as other multi-task learning algorithms. We also examined the performance of algorithms across different parameter settings that control for sparsity as well as for sharing information. We found that the algorithms were generally robust to the setting of sharing and more sensitive to the extent of sparsity. However, multi-task learning algorithms generally outperformed single-task learning algorithms indicating that this is a useful direction for methodological development for GRN inference from single cell

omic datasets. Importantly, single-task learning infers very different networks that makes it challenging to study transitions across the networks.

Once GRNs are inferred across multiple cell types, the next challenge is to examine which components of the GRNs change along the lineage. We developed two complimentary techniques to study dynamics. Our k-means edge clustering method was able to find regulatory connections that were unique to each cell cluster, while our topic model-based dynamic network analysis highlighted subnetworks that were activated or deactivated along the lineage. We applied our tools to study GRN dynamics in hematopoietic cell differentiation and reprogramming from mouse embryonic fibroblasts to embryonic stem cells. We found that both these systems exhibited different dynamics, with the reprogramming system exhibiting more edges shared across populations compared to the hematopoietic system which identified most edges as cell cluster-specific. In both systems, our analysis identified known and novel regulators. For example, in the reprogramming system, we found that cells that were closer to the end point pluripotent state already had an Esrrb-centered GRN component active. In contrast, for cells that were on an alternate trajectory had several oncogenes such as Wt1 as key regulators. In the hematopoietic system, our analysis examined immuno-phenotypically similar populations by identifying different set of hematopoietic regulators associated with such populations.

scMTNI currently assumes that the input lineage structure is accurate. However, lineage construction, especially from integrated scRNA-seq and scATAC-seq datasets is a challenging problem. One direction of future work is to assume the initial lineage structure is inaccurate and incorporate the refinement of the lineage structure as part of the GRN inference procedure. A second direction of work is to model more fine-grained transitions within each cell population, for example using RNA velocity or pseudotime, which will complement the coarse-grained dynamics that scMTNI currently handles. Studies from bulk RNA-seq data have shown that estimating hidden transcription factor activity (TFA)[56] can further improve the performance of network inference. Thus, another direction of future work is to estimate hidden TFA and incorporate these to improve the accuracy of the inferred networks. Finally, SCENIC performs very well among the single-task learning algorithms, which is likely because of its regression-tree based model that captures non-linear dependencies and is less prone to the sparsity of the dataset. While scMTNI's stability selection framework can capture some non-linearities, another direction of future work is to extend scMTNI to model more non-lineage dependencies.

In summary, scMTNI is a tool to infer cell type-specific regulatory networks and their dynamics on a cell lineage which combines scRNA-seq and scATAC-seq data. As single cell multi-omic datasets become increasingly available, we expect scMTNI to be broadly applicable to predict GRNs and identify

372 important regulators associated with regulatory network dynamics across cell types in diverse cell-fate
373 specification processes.

Methods

Single-cell Multi-Task Network Inference (scMTNI)

Single-cell Multi-Task Network Inference (scMTNI) is a probabilistic graphical model-based approach that uses multi-task learning to infer gene regulatory networks for cell types related on a cell lineage tree (**Figure 1**). We define a cell type to be a group of cells with similar transcriptome and accessibility levels as defined by existing cell clustering methods. Each task learns the gene regulatory network (GRN), $\mathbf{G}^{(d)}$ for each cell type or cell cluster d. Given cell type-specific datasets for M cell types, $\boldsymbol{\mathcal{D}} = \{D^{(1)}, \cdots, D^{(M)}\}$, our task is to find the set of graphs $\boldsymbol{\mathcal{G}} = \{\mathbf{G}^{(1)}, \cdots, \mathbf{G}^{(M)}\}$ and parameters $\boldsymbol{\Theta} = \{\theta^{(1)}, \cdots, \theta^{(M)}\}$ for each of the cell types. $\mathbf{G}^{(d)}$ is modeled as a dependency network[21], a class of probabilistic graphical models for inferring directed, predictive relationships among random variables (regulators and genes). Each gene is modeled as a random variable $X_i^{(d)}$ which encodes the expression level of gene i in each cell. A conditional probability distribution $P(X_i^{(d)}|\mathbf{R}_i^{(d)})$ models the relationship between gene i and its set of regulators, $\mathbf{R}_i^{(d)}$ in cell type d. In a dependency network, GRN inference entails estimating the regulators $\mathbf{R}_i^{(d)}$ for each gene i in each cell type d. To enable joint learning of these cell type-specific networks our goal is to find the set $\boldsymbol{\mathcal{G}} = \{\mathbf{G}^{(1)}, \cdots, \mathbf{G}^{(M)}\}$ and parameters $\boldsymbol{\Theta} = \{\theta^{(1)}, \cdots, \theta^{(M)}\}$ by estimating the posterior distribution of these two sets and finding their maximum a posteriori values:

$$P(\boldsymbol{\mathcal{G}}, \boldsymbol{\Theta}|\boldsymbol{\mathcal{D}}) \propto P(\boldsymbol{\mathcal{D}}|\boldsymbol{\mathcal{G}}, \boldsymbol{\Theta}) P(\boldsymbol{\Theta}|\boldsymbol{\mathcal{G}}) P(\boldsymbol{\mathcal{G}}) \tag{1}$$

$P(\boldsymbol{\mathcal{D}}|\boldsymbol{\mathcal{G}}, \boldsymbol{\Theta})$ is the data likelihood, expanded as $\prod_d P(\boldsymbol{D}^{(d)}|\boldsymbol{G}^{(d)}, \theta^{(d)})$. In a dependency network, pseudo likelihood[21] is used to approximate the data likelihood for each cell type, defined as the products of the conditional distribution of each random variable $X_i^{(d)}$ given its neighbor set $\boldsymbol{R}_i^{(d)}$ in cell type d, $P(X_i^{(d)}|\boldsymbol{R}_i^{(d)}, \theta_i^{(d)})$. Thus, the likelihood can be written as:

$$P(\boldsymbol{\mathcal{D}}|\boldsymbol{\mathcal{G}}, \boldsymbol{\Theta}) \propto \prod_{d \in \{1,\ldots,M\}} \prod_{i \in \{1,\ldots,N\}} P(X_i^{(d)}|\boldsymbol{R}_i^{(d)}, \theta_i^{(d)}) \tag{2}$$

Given the neighbor set $\boldsymbol{R}_i^{(d)}$, the above quantity can be computed efficiently. We assume that each variable $X_i^{(d)}$ and its neighbor set $\boldsymbol{R}_i^{(d)}$ in cell type d are from a multi-variate Gaussian distribution. Thus, $P(X_i^{(d)}|\boldsymbol{R}_i^{(d)}, \theta_i^{(d)})$ can be modeled using a conditional Gaussian distribution with mean $\mu_{X_i^d|R_i^d}$ and variance $\sigma^2_{X_i^d|R_i^d}$ which can be estimated in closed form. $\boldsymbol{R}_i^{(d)}$ is selected from the input list of

regulators using a greedy search algorithm, executed in parallel across all cell types (See **Supplementary Methods**). The second term $P(\boldsymbol{\Theta}|\boldsymbol{\mathcal{G}})$ in **Equation** (1) is estimated using the maximum likelihood settings of the parameters. The third term $P(\boldsymbol{\mathcal{G}}) = P(\mathbf{G}^{(1)}, \cdots, \mathbf{G}^{(M)})$ in the objective function is the structure prior and is defined in a way to capture the state of an edge across all cell types modeled, where $\boldsymbol{\mathcal{G}} = \{\mathbf{G}^{(1)}, \cdots, \mathbf{G}^{(M)}\}$. We assume that $P(\boldsymbol{\mathcal{G}})$ is composed of two priors, one is the cell-type specific prior $P(\boldsymbol{T})$, where $\boldsymbol{T} = \{T^{(1)}, ..., T^{(M)}\}$, and the other one is a cell lineage structure prior $P(\boldsymbol{S})$ which captures the similarity between related cell types along the cell lineage tree, where $\boldsymbol{S} = \{S^{(1)}, ..., S^{(M)}\}$.

$P(\boldsymbol{T})$ is the cell-type specific prior, which decomposes over a product of cell-type specific graphs: $P(T^{(1)}, ..., T^{(M)}) = \prod_{d=1}^{M} P(T^{(d)})$. The $P(T^{(d)})$ decomposes over a product of individual edge configurations, $P(I_{u,v}^{(d)})$, where $I_{u,v}^{(d)}$ is an indicator function that represents whether there exists an edge between regulator u to target gene v in cell type d, $X_u \rightarrow X_v$ as follows:

$$I_{u,v}^{(d)} = \begin{cases} 1, & \text{if there is an edge from } u \text{ to } v \text{ in cell type } d, \\ 0, & \text{otherwise.} \end{cases}$$

As in Roy et al[57], we model the prior probability using a logistic function:

$$P\big(I_{u,v}^{(d)} = 1\big) = \frac{1}{1 + e^{-(\beta_0 + \beta_1 * m_{uv}^{(d)})}} \tag{3}$$

The β_0 parameter is a sparsity prior that controls the penalty of adding of a new edge to the network, which takes a negative value ($\beta_0 < 0$). A smaller value of β_0 will result in a higher penalty on adding new edges and will therefore infer sparser networks. The β_1 parameter controls how strongly motifs are incorporated as prior ($\beta_1 \geq 0$). A higher value of β_1 will result in motif presence being valued more strongly to select an edge. β_1 is set to 0 when there is no cell type-specific motif information available. $m_{uv}^{(d)}$ is the weight of the edge from regulator u to target v in the prior network and is computed based on the motif instance score if gene v has a motif of regulator u in its promoter region that overlaps an ATAC-seq peak. Thus, we have

$$P(\boldsymbol{T}) = \prod_{d=1}^{M} P(T^{(d)}) = \prod_{d=1}^{M} \prod_{u,v;u \neq v} P(I_{u,v}^{(d)}) \tag{4}$$

The cell lineage structure prior $P(\boldsymbol{S})$ is constructed to make use of multi-task learning. We define that $P(S^{(1)}, ..., S^{(M)})$ can be rewritten as a product over a set of edges between regulators and target genes: $\prod_{u,v;u \neq v} P(I_{u,v}^{(1)}, ..., I_{u,v}^{(M)})$. Under the assumption that the prior probability of the edge state in

one cell type is only dependent upon its state in the predecessor cell type, we have:

$$P(\boldsymbol{S}) = \prod_{u,v;u\neq v} P(I_{u,v}^{(1)}, ..., I_{u,v}^{(M)}) = \prod_{u,v;u\neq v} \prod_{d\in\{1,...,M\}} P(I_{u,v}^{(d)}|I_{u,v}^{pa(d)})P(I_{u,v}^{(r)}), \quad (5)$$

where $pa(d)$ denotes the predecessor cell of cell type d on the cell lineage tree and r denotes the starting root cell. $P(I_{u,v}^{(d)}|I_{u,v}^{pa(d)})$ is a measure of overall regulatory gain and loss of regulatory connections between related cell types, and is assumed to be the same across the set of edges. Thus, it can specified by three parameters: the probability of gaining a regulatory edge in the starting cell, $p_r = P(I_{u,v}^{(r)})$, the probability of gaining a regulatory edge in cell type d given that the edge does not exist in its predecessor cell $p_g^{(d)} = P(I_{u,v}^{(d)} = 1|I_{u,v}^{pa(d)} = 0)$, and the probability of maintaining a regulatory edge in cell type d, given its presence in its predecessor cell $p_m^{(d)} = P(I_{u,v}^{(d)} = 1|I_{u,v}^{pa(d)} = 1)$. These parameters of the priors can be set by the user or estimated empirically by analyzing different configurations and selecting those values with the best agreement with existing biological knowledge of the system. scMTNI uses a greedy score-based structure learning algorithm. Please refer to **Supplementary Methods** for details.

Input Datasets

Simulated Datasets

To benchmark the performance of different multi-task and single-task learning algorithms, we simulated single cell expression data from a lineage resembling a linear differentiation process for three cell types (**Figure 2A**). We simulated network dynamics on a lineage tree and controlled the extent of similarity with the three prior parameters: p_r, the probability of having an edge in the starting/root cell type; $p_g^{(d)}$, the probability of gaining an edge in cell type d that is not in the predecessor cell type; $p_m^{(d)}$, the probability of maintaining an edge in cell type d from the predecessor cell type. We set $p_r = 0.5, p_g^{(d)} = 0.4$ and $p_m^{(d)} = 0.7$ or 0.8 and simulated three networks from a linear lineage tree for each of the three cell types, each with 15 regulators and 65 genes. Next, we applied BoolODE on the simulated gene regulatory networks and generated single cell expression data for 2000 cells for each cell type. To mimic the dropouts in the scRNA-seq data, we added 80% sparsity uniformly to all genes on the simulation data. We refer to this simulated dataset as data 1, consisting of 65 genes and 2,000 cells for three cell types. We generated smaller sample sizes of these datasets, data 2 and data 3 by downsampling data 1 to 1,000 cells (data 2) and 200 cells (data 3). We applied each of the algorithms on these three datasets within a stability selection framework and evaluated their performance based on AUPR and F-score as

445 described in the **Evaluation** section.

446 ## Human hematopoietic differentiation data

447 Buenrostro et al.[41] measured single-cell accessibility (scATAC-seq) and single-cell RNA sequencing
448 (scRNA-seq) data to study the regulatory dynamics during human hematopoietic differentiation for mul-
449 tiple immuno-phenotypic cell types: hematopoietic stem cells (HSCs), common myeloid progenitors
450 (CMPs) and granulocyte-macrophage progenitors (GMPs) and Monocytes (Monos). We downloaded
451 fragment files for the scATAC-seq data and processed scRNA-seq data for each cell type. For the
452 scATAC-seq data we mapped the fragments into 23,347,540 bins with length of 1000bp. Next, we
453 mapped 1kb bins to the nearest gene and extracted cells with cell barcodes labeled as HSC, CMP, GMP
454 and Mono cells. Next, we filtered out genes with sum of counts in all samples less than 100 producing
455 a processed scATAC-seq dataset with 54,344 genes and 1,315 cells across the four cell types. We ex-
456 tracted the count matrix of scRNA-seq from these four cell types. After filtering out genes with non-zero
457 expression in less than 5 cells, the scRNA-seq data had 12,558 genes and 4,165 cells. We normalized
458 the count matrix for depth and variance stabilization based on the pagoda pipeline[58]. We kept 12,393
459 common genes between scATAC-seq and scRNA-seq data and applied LIGER[22] to define integrated cell
460 populations. We applied LIGER with $k \in 8, 10, 12, 15, 20$ and found 10 cell subpopulations to be most
461 appropriate. C8 was mainly composed of HSCs, C6 was mainly composed of GMP cells, C7 was mainly
462 CMP0 cells, C1 was composed of Mono cells, and the rest clusters were a combination of several cell
463 types. C5 had too few RNA cells (22 cells) so we excluded it from further analysis. Since the composi-
464 tion of C1 (73 cells) and C4 (37 cells) are very similar, mainly GMP and Mono cells, we combined these
465 two clusters as C1. We inferred a cell lineage tree from the 8 cell clusters using a minimal spanning tree
466 approach (python package `scipy.sparse.csgraph`).

467 To derive the prior network for each cell cluster we created cluster-specific bam files from the
468 scATAC-seq data using the LIGER clusters. We pooled these bam files to generate pseudo bulk accessi-
469 bility coverage and applied MACS2 to identify scATAC-seq peaks for each cell cluster[59]. We obtained
470 sequence-specific motifs from the Cis-BP database[60] and used the script `pwmmatch.exact.r` avail-
471 able from the PIQ toolkit[61] to identify significant motif instances genome-wide using the human genome
472 assembly of hg19. We mapped motifs to each scATAC-seq peak and mapped the peak to a gene if it was
473 within $\pm$5000bp of the transcription start site (TSS) of a gene. In this case, we connect motifs to TSS that
474 are mapped to the same scATAC-seq peak. We used the max motif score from `pwmmatch.exact.r`
475 for each motif-TSS pair and took the maximum value among all TSSs of a gene as the value for each

motif-gene pair. The motif instance score is the log ratio of the PWM to a uniform background. Finally, to generate the edge weight for each TF-gene pair, we used the max score among all motifs mapped to the same TF. To normalize the edge weights across TFs, we converted these weights into percentile scores and selected the top 20% of edges as prior edges.

Mouse reprogramming data

We generated a novel scATAC-seq time course dataset for cellular reprogramming from mouse embryonic fibroblast (MEF) reprogramming to induced pluripotent cells (iPSC). The dataset contains had a total of 6 time points corresponding to the starting MEF, the end pluripotent state (mESC), and four intermediate timepoints of day3, day6, day9 and day12. We downloaded scRNA-seq datasets (GEO: GSE108222) for the same time points from Tran et al[62]. The scATAC-seq data was first processed through CellRanger ATAC pipeline to provide the `frags.txt` file. We binned the genome at non-overlapping 1kb bin and computed the number of fragments mapped to each 1kb bin. Next, we mapped 1kb bins to the nearest gene for all of the samples. For scRNA-seq data, we concatenated the expression data from two replicates at each time point and normalized the concatenated matrix for depth and variance stabilization based on the pagoda pipeline[58]. Next, for each time point, we removed genes with expression in less than 5 cells. We took the union of genes among all time points and concatenated the expression data across all time points as our final scRNA-seq data matrix. The processed scATAC-seq data contains 25,824 genes and 30,344 cells. The processed scRNA-seq dataset contains 14,953 genes and 3,460 cells. We had a total of 11,926 genes in common between the two datasets, which were used for downstream analysis. We applied LIGER with $k \in 8, 10, 12, 15, 20$ and found $k = 8$ to provide the optimal clustering of the scRNA-seq and scATAC-seq data determined based on the clustering of the accessibility and transcriptome of the MEF and ESC time points. We used the mean expression profiles across samples of these cell clusters and computed the Euclidean distance between every cell clusters. Then, we inferred a minimal spanning tree using the distance matrix and used it as the cell lineage tree using `scipy.sparse.csgraph` in python. The prior motif was generated in the same way as for the hematopoeisis differentiation dataset using motifs for mouse from the CisBP database[60]. We used mouse genome mm10 for this analysis.

Application of network inference algorithms on simulated datasets

We used the simulated datasets to perform extensive benchmarking of the different network inference algorithms. We also used this dataset to study the sensitivity of the algorithms to the different parameter settings. Below we describe each of the algorithms as well as the parameters used for each of the algorithms for the simulated datasets. For all three simulation datasets, we applied all algorithms other than SCENIC within a stability selection framework to estimate the confidence score for each edge in the predicted networks. For stability selection we subsampled each dataset 20 times randomly using half of the cells and all genes. SCENIC has its own internal sub-sampling and directly outputs the edge confidence.

scMTNI. scMTNI has five hyper-parameters: p_r, probability of having an edge in the starting cell type; $p_g^{(d)}$, probability of gaining an edge in a child cell type d; $p_m^{(d)}$ the probability of maintaining an edge in d from its immediate predecessor cell type; a sparsity penalty β_0, that controls penalty for adding edges; β_1, that controls the strength of incorporating prior network. We tried different configurations of the hyper-parameters: $p_r \in \{0.1, 0.15, 0.2, 0.25, 0.3, 0.35, 0.4, 0.45, 0.5\}$, and $p_g^{(d)} \in \{0.05, 0.1, 0.15, 0.2, 0.25, 0.3, 0.35, 0.4, 0.45\}$, and $p_m^{(d)} \in \{0.55, 0.6, 0.65, 0.7, 0.75, 0.8, 0.85, 0.9\}$, $\beta_0 \in \{-0.005, -0.01,-0.05, -0.1, -0.5\}$. β_1 was set to 0 as there is no prior network in the simulations. If the size of the predicted network for a parameter setting was smaller than the size of the simulated network, we disregarded this parameter setting for comparison. We used the area under the precision-recall curve (AUPR) to compare the scMTNI inferred networks to simulated networks. We also computed F-score on top K edges ranked by the confidence score (where K is the number of edges in the simulated network, see **Table 1**). Overall performance of scMTNI was stable across different parameter configurations (**Supplementary Figure 17**, **Supplementary Methods**). To compare against methods, we used values from the best parameter settings for each dataset and cell type as well as all parameter settings (**Supplementary Figure 1,2**).

MRTLE. Multi-species regulatory network learning (MRTLE)[24] is a probabilistic graphical model-based algorithm that uses phylogenetic structure, transcriptomic data for multiple species, and sequence-specific motifs to infer the genome-scale regulatory networks across these species simultaneously. It was developed for bulk transcriptomic data. It uses a dependency network model to specify the directed relationship among regulators to target genes. Sequence-specific motif instances can be incorporated as prior knowledge to favor edge supported with presence of motifs. The multi-task learning framework is em-

bedded in the phylogenetic prior, which captures the evolutionary dynamics of regulatory edge gain and loss guided by the phylogenetic structure. The MRTLE algorithm has four parameters: p_g, the probability of gaining an edge in a child species s that is not in the ancestor species; p_m, the probability of maintaining an edge in a species s given that is also in s's immediate ancestor of s; β_0, a sparsity penalty that controls penalty for adding edges, and a penalty β_1 that controls the strength of motif prior. In the simulation case, we examined different parameter configurations: $p_g \in \{0.05,0.1,0.15,0.2,0.3,0.4\}$, $p_m \in \{0.5,0.55, 0.6, 0.65, 0.7, 0.75, 0.8, 0.85\}$, $\beta_0 \in \{-0.005,-0.01, -0.05,- 0.1, -0.5, -1\}$. β_1 was set to 0. The overall performance of MRTLE was stable across different parameter configurations (**Supplementary Figure 18**). Similar to scMTNI, we used the AUPR and F-score of top K edges to select the best parameter setting. The best parameter setting and all parameter settings were used to compare against other algorithms.

GNAT. The GNAT[25] algorithm uses a hierarchy of tissues to share information between related tissue and infers tissue-specific gene co-expression networks. It was developed for bulk transcriptomic data. GNAT models each network using a Gaussian Markov Random Field (GMRF). It has two parameters: the L_1 penalty λ_s that controls the sparsity of the network, and the L_2 penalty λ_p that encourage the precision matrix of children to be similar to its parent precision matrix. It initially learns a co-expression network for each leaf tissue. Then it infers the networks in internal nodes using the networks in the leaf nodes and updates the networks in leaf nodes for several iterations until convergence. Since GNAT learns undirected networks, we transformed them to directed networks by adding edges from a regulator to a target. If the nodes of an edge are both candidate regulators, we output the edge in both directions. We tried different parameter configurations of λ_s and λ_p. For data 1 (n=2000), λ_s were set to $\{30, 31, 32,..., 37\}$, and λ_p were set to $\{30, 31, 32,..., 40\}$. For data 2 (n=1000), λ_s were set to $\{18, 19,..., 22\}$, and λ_p were set to $\{18, 19,..., 25\}$. For data 3 (n=200), λ_s were set to $\{5, 6, 7, 8\}$, and λ_p were set to $\{5, 6, 7, 8\}$. We found that λ_s dominates the performance and under the same λ_s, changing λ_p does not change the performance a lot (**Supplementary Figure 19**). If the size of the predicted network for a parameter setting is smaller than the size of the simulated network, we removed this parameter setting. In this case, the ranges of λ_s and λ_p are slightly different and varying across different datasets. We used AUPR and F-score of top K edges to select the best parameter settings. We compared the algorithms using these and all parameter settings.

Ontogenet. The Ontogenet[26] algorithm was developed to reconstruct lineage-specific regulatory networks using cell type-specific gene expression data across cell lineages. It was developed for bulk transcriptomic data. To infer the regulatory networks for each cell type, it uses a fused LASSO framework combined with an additional L_2 penalty. The L_1 penalty is introduced to control the sparsity of regulators, while the L_2 penalty is used to select correlated predictors. The multi-task learning comes in the fused LASSO framework with additional L_1 penalty on the difference of the regression weight of related cell types, which encourage the consistency of regulatory programs between related cell types. Ontogenet was applied on the same subsample of the three simulation datasets within a stability selection framework to estimate the confidence score for each edge in the networks. The Ontogenet algorithm has three parameters: the L_1 penalty λ that controls the sparsity of the network, the L_2 penalty κ that handles correlated predictors, and γ that encourage the similarity of regulatory programs between related cell types. We tried different parameter configurations of λ, γ and κ. For data 1 (n=2000), λ were set to $\{$1000,1250,1500,1750,2000,2250,2500$\}$, and γ were set to $\{$1000,1250,1500,1750,2000,2250,2500$\}$. For data 2 (n=1000), λ were set to $\{$500,1000,2000,3000$\}$, and γ were set to $\{$500,1000,2000,3000$\}$. For data 3 (n=200), λ were set to $\{$475,500,525$\}$, and γ were set to $\{$475,500,525$\}$. κ was set to $\{$1, 5, 10$\}$ for each of the datasets. We found that λ and γ dominate the performance and while changing κ does not change the performance significantly (**Supplementary Figure 20**). If the size of the predicted network for a parameter setting is smaller than the size of the simulated network, we removed this parameter setting. The ranges of λ and γ are slightly different and varying across different datasets in order to infer similarly sized networks for different datasets. We used AUPR and F-score of top K edges to select the best parameter settings. We compared the algorithms using these and all parameter settings.

AMuSR. The Inferelator-AMuSR[27] algorithm uses sparse block-sparse regression to estimates the activities of transcription factors and infer gene regulatory networks from expression datasets. The multi-task learning approach decomposes the model coefficients matrix into a dataset-specific component using a sparse penalty and a conserved component using a block-sparse penalty to capture both conserved interactions and dataset-unique interactions. It is able to incorporate prior knowledge from multiple resources and robust to false interactions in the prior network. For our simulation setting, we applied AMuSR without TFA estimation by setting worker.set_tfa(tfa_driver=False) in the SingleCellWorkflow from Inferelator 3.0 package. To be comparable across different algorithms, AMuSR was applied on the same subsample of the three simulation datasets within a stability selection framework to estimate the confidence score for each edge in the AMuSR networks. The AMuSR algorithm has two sparsity

parameters: λ_s that controls the sparsity of the network for each dataset, the block-sparse penalty λ_b that controls the sparsity of the conserved network across all datasets. AMuSR has its own parameter selection framework (see[27] for details) and uses extended Bayesian information criterion (EBIC) to select the optimal (λ_s, λ_b). We additionally externally tuned the parameters by setting c to {0.01, 0.02154435, 0.04641589, 0.1,0.21544347,0.46415888,1., 2.15443469, 4.64158883,10 } and set $\lambda_b = c * \sqrt{\frac{d*log(p)}{n}}$ as suggested in the paper, where d is the number of cell types and n is the number of samples and p is the number of genes. However, by setting λ_b to 0 and λ_s to 0, we found that the inferred networks are too sparse with 7-100 edges for data 1, and 71-129 edges for data 2. We kept two settings for AMuSR, one using our criteria to select the best setting based on AUPR and F-scores among different c settings (AMuSR_tuned) and another version using AMuSR's default optimal parameter selection (AMuSR_default). We computed AUPR and F-score of top K edges (where K is the number of edges in the simulated network) for AMuSR inferred networks with optimal parameter settings for comparison with other algorithms. We compared the algorithms using the optimal and all parameter settings.

INDEP. The INDEP algorithm is the single-task framework of scMTNI which does not have the prior for sharing information across cell types and infers a regulatory network for each cell type independently. It also models each network using a dependency network as scMTNI. INDEP learns the graphs for each cell type using a greedy graph learning algorithm with a score-based search, where the score contains only the data likelihood. At each iteration, the algorithm computes the change in data likelihood score[21] for all candidate regulators for each target gene, selects the best regulator for the target gene and adds this (regulator, target) edge to the current graph. INDEP has two parameters in the model: a sparsity penalty β_0 that controls penalty for adding edges, and a penalty β_1 that controls the strength of motif prior. In the simulation case, β_0 were set to {-0.005,-0.01, -0.05, -0.1, -0.5, -1}, and β_1 were set to 0. AUPR and F-score of top K edges were used to select the best parameter settings (**Supplementary Figure 21**). If the size of the predicted network for a parameter setting is smaller than the size of the simulated network, we removed this parameter setting. As above, we compared INDEP to other algorithms using best and all parameter settings for a dataset.

LASSO. The LASSO regression is linear regression with L_1 regularization. For each gene, we use the expression profiles of candidate regulators to predict the expression profiles of this gene. The regulators with non-zero coefficients are inferred as the regulators for this gene and these edges are added to the gene regulatory network. We used matlab implementation of the LASSO regression. Similarly to

scMTNI and MRTLE, LASSO was run on the same subsample of the three simulation datasets within a stability selection framework to estimate the confidence score for each edge in the networks. LASSO has only the L_1 penalty λ that controls the sparsity of the network. In the simulation case, λ were set to $\{0.01, 0.02, 0.03, 0.04, 0.05, 0.06\}$. AUPR and F-score of top K edges were used to select the best parameter settings (**Supplementary Figure 22**). If the size of the predicted network for a parameter setting is smaller than the size of the simulated network, we removed this parameter setting. We compared LASSO to other algorithms using the best and all parameter settings.

SCENIC. The SCENIC[29] algorithm uses GENIE3 or GRNBoost2 to infer TF-target relationships available as part of the Arboreto framework[63]. We used the GRNBoost2 algorithm with default parameters for network inference. SCENIC is based on ensemble models with its own bootstrapping and hence was directly applied to each cell type-specific dataset in the simulation. SCENIC uses the feature importance score of each edge to rank the edges in the inferred network. We computed AUPR and F-score of top K edges (where K is the number of edges in the simulated network) for SCENIC inferred networks for comparison with other algorithms.

Application of network inference algorithms to cellular reprogramming data

We applied scMTNI, scMTNI+prior, INDEP, INDEP+prior and SCENIC to this dataset. scMTNI and INDEP algorithms were applied within a stability selection framework to estimate edge confidence. SCENIC has its own subsampling framework which can estimate an edge importance. In the stability selection framework, we subsampled the data 50 times, each with 12,216 genes and $\frac{2}{3}$ of the cells, applied the algorithms to each subsample and used the inferred networks to estimate the confidence score for each TF-target edge in the predicted networks. In both scMTNI and scMTNI+prior, we used the following hyper-parameter settings for the lineage structure prior $p_r = 0.2$, $p_g^{(d)} = 0.2$ and $p_m^{(d)} = 0.8$. For the sparsity prior we set $\beta_0 = -0.9$ for scMTNI, and $\beta_0 \in \{-0.9, -2, -3, -4\}$ for scMTNI+prior. To generate prior network, we used the matched scATAC-seq clusters to obtain TF-target prior interactions for each scRNA-seq cluster. For scMTNI+prior which uses the scATAC-seq prior, we set $\beta_1 \in \{2, 4\}$. INDEP and INDEP+prior were applied on the same subsampled data followed by edge confidence estimation. We used the same settings for β_0 and β_1 for INDEP as scMTNI. Final results of scMTNI+prior are using $\beta_0 = -4$ and $\beta_1 = 4$, which was determined by the distribution of edges at different confidences. Final results for INDEP+prior are using $\beta_0 = -4$ and $\beta_1 = -4$. SCENIC was applied to the entire dataset with default parameter settings.

Application of network inference algorithms to human hematopoietic differentiation data

We used a similar workflow for the human hematopoietic differentiation dataset as the reprogramming system. We subsampled the scRNA-seq data for each cell cluster 50 times, each with 11,994 genes and $\frac{2}{3}$ of the cells, and applied scMTNI, scMTNI+prior, INDEP, INDEP+prior on each subsample to estimate the edge confidence of the GRNs. For scMTNI and scMTNI+prior, the lineage structure prior parameters were set as follows: $p_r = 0.2$, $p_g^{(d)} = 0.2$, $p_m^{(d)} = 0.8$. The sparsity prior β_0 was set to -0.9 for scMTNI. For scMTNI+prior, the sparsity prior was set $\beta_0 \in \{-0.9, -2, -3, -4\}$ and $\beta_1 \in \{2, 4\}$. For INDEP and INDEP+prior, we used the same settings for β_0 and β_1 for as scMTNI and scMTNI+prior respectively. Final results of scMTNI+prior are with $\beta_0 = -4$ and $\beta_1 = 4$ and final results for INDEP+prior are using $\beta_0 = -4$ and $\beta_1 = -4$. SCENIC was applied to the entire dataset with default parameter settings.

Evaluation

Gold standard datasets

To evaluate the predicted networks of different inference algorithms on real data, we downloaded and processed several gold standard datasets (**Tables 2, 3**). For human hematopoietic cell types, we have five gold standard datasets. Two gold standard datasets were a ChIP-based (Cus_ChIP) and a regulator knock down-based (Cus_KO) gold standard dataset in GM12878 lymphoblastoid cell line downloaded from Cusanovich et al[43]. For the knockout dataset, we had TF-target relationships at two p-value thresholds, 0.01 and 0.05. We used the one at 0.01 to have a more stringent gold standard. The third gold standard was from human hematopoietic cell types from the UniBind database (`https://unibind.uio.no/`)[42], which has high confidence TF binding site predictions from ChIP-seq experiments. To obtain the TF-gene network, we mapped TF binding sites to the nearest gene if there is overlap between the TF binding sites and the promoter of the gene define by ± 5000bp. If multiple ChIP-seq datasets were available for the same TF in a given cell type, we took the union of TF-gene edges for the same cell type. We took the union of these individual cell type-specific gold standards to create our Unibind gold standard (UniBind). Finally, we took the intersection of the ChIP-based gold standards with the knockdown based gold standards, Unibind+Cus_KO and CusChIP+Cus_KO to produce the fourth and fifth gold standards. The statistics of the gold standard datasets are provided in **Table 3**.

For mouse reprogramming study we curated multiple experimentally derived networks of regulatory interactions from the literature and existing databases. The statistics of the gold standard datasets are

provided in **Table 2**. One of these experiments is ChIP based gold standard (referred to as "ChIP") from ESCAPE or ENCODE databases[31,32], which contains ChIP-chip or ChIP-seq experiments in mouse ESCs. Another is knock-down based gold standard (referred to as "Perturb"), which is derived from regulator perturbation followed by global transcriptome profiling[31,33]. We took a union of the networks from LOGOF (loss or gain of function) based gold standard networks from ESCAPE database[31] and the networks from Nishiyama et al[33] as the perturbation interactions. Finally, we took the intersection of the interactions between ChIP and knock-down based gold standard to create the third gold standard network referred to as "ChIP+Perturb".

Area Under the Precision Recall Curve

To evaluate the performance of scMTNI and other algorithms, we compared the inferred networks to the simulated networks or interactions from the gold standard datasets based on Area under the precision recall curve (AUPR). Edge weights for all but the SCENIC algorithm were obtained using stability selection. In our stability selection framework, we generated N random subsamples of the data, inferred a network for each subsample, and calculated a confidence score for each edge as the fraction of how many times this edge was present in the inferred networks across all subsamples. Next, we ranked the edges by the confidence score and estimated precision and recall at different confidence thresholds ranging from 0 to 1. Precision P is defined as the fraction of the number of edges that are true positives among the total number of predicted edges. Recall R is defined as the fraction of the number of edges that are true positives among the total number of true edges. Then, we plotted the precision recall curve and estimated the area under this curve using the AUCCalculator package developed by Davis et al.[64]. The area under the precision recall curve is computed as an overall assessment of the inferred networks compared to "true" networks. The higher AUPR, the better the performance is. For the real scRNA-seq datasets, we filtered the inferred networks to include TFs and targets that were in the gold standard.

F-score

While AUPR uses a ranking of the edges, F-score is a metric to compare a set of predicted edges to a set of "true" edges. F-score is defined as the harmonic mean of the precision (P) and recall (R),

$$\text{F-score} = \frac{2*\text{P}*\text{R}}{\text{P}+\text{R}}$$

F-score enables us to control for the number of edges across network inference algorithms as these can vary significantly across algorithms. To control for number of edges in the predicted networks, we ranked the predicted network by the confidence score or edge weight, selected top K edges and computed F-score compared to simulated networks or gold standard networks. K in the simulated datasets corresponded to the size of the simulated networks. For the real datasets, we considered top 500, 1000, 2000 edges. We obtained the top K edges after filtering the inferred networks based on the TFs and targets in the gold standard networks.

Examining network dynamics on cell lineages

We used several global and subnetwork-level methods to examine how regulatory networks change on a cell lineage. These include F-score based comparison of all pairs of networks on the lineage, k-means based edge clustering and Latent Dirichlet Allocation (LDA).

F-score based analysis of inferred network change along cell lineage tree

To examine the overall conservation and divergence between the inferred cell type-specific networks along the cell lineage tree, we computed F-score on the predicted networks between each pair of cell types and applied hierarchical clustering on the inferred networks based on the F-score. To compute F-score, we selected top X edges ranked by confidence score to obtain a reliable network for each cell type, where X was close to the median of the number of 80% confident edges across all cell types. This was 4k in the mouse reprogramming dataset and 5k in the hematopoietic differentiation dataset. We visualized the dendrogram obtained from the hierarchical clustering and compared this to the original cell lineage tree.

k-means based edge clustering

For each cell cluster, we selected top K edges, where K was close to the median number of edges with at least 80% confidence across all cell types. This corresponded to 4k edges for the mosue reprogramming dataset and 5k edges for the hematopoietic differentiation dataset. We merged the confidence score of each edge across all cell types as an edge by cell type matrix, each entry corresponding to the edge confidence and with as many edges as in the union of top K edges from any cell type. We applied k-means clustering on this matrix to find subnetworks with different patterns of conservation. We tried a range of number of clusters and selected the one that has the highest silhouette coefficient.

Latent Dirichlet Allocation (LDA) model for regulatory network rewiring

We adopted Latent Dirichlet Allocation (LDA) to examine subnetwork level rewiring as shown in TopicNet[36]. LDA was originally developed to cluster documents based on their word distributions. Each document, i is assumed to have a certain composition of topics, as captured by a θ_i parameter and each topic, k, is assumed to have a specific distribution of words as captured by a φ_k parameter. In the application of LDA to a regulatory network, we first concatenated the TF by target network across cell types to have as many rows as there are TFs times the number of cell types. Each TF in a cell type is treated as a document and its targets are treated as words in the document. The topic distribution for all documents constitutes a $M \times K$ matrix for document-topic distribution, where M is the total number of TFs in any of the networks and K is the total number of topics. The distribution of words (genes) in each topic is captured by $K \times V$ matrix for V genes. Each gene can be assigned to a topic based on its maximum probability across topics. We applied LDA model to the 80% confidence networks of all cell clusters inferred from scMTNI with 10 or 15 topics and found 10 topics to be suitable for both datasets. We extracted the subnetworks in each cell type associated with each topic by obtaining the induced graph for the genes and regulators associated with each topic and visualized the giant components of each network to identify change across cell clusters within the same topic.

For the mouse reprogramming dataset, we used the results of LDA application with 10 topics on the 80% confidence networks of all cell clusters (**Supplementary Figure 5, 6, 7**). To interpret the topics in each cell type, we tested the genes in the cell type-specific subnetwork for each topic for enrichment of gene ontology (GO)[65] processes using a hypergeometric test with FDR correction. We used an FDR $<$0.01 to determine significant enrichment (**Supplementary Figure 8**). For the hematopoiesis dataset, we also used LDA results with 10 topics on the 80% confidence networks of all cell clusters (**Supplementary Figure 13, 14, 15**) and used FDR $<$0.01 to determine significantly enriched terms (**Supplementary Figure 16**).

Data and code availability

Pre-processed datasets are available at scMTNI Supplementary website at `https://github.com/Roy-lab/scMTNI`. The reprogramming scATAC-seq dataset has been deposited to Gene Expression Omnibus (GEO). The scMTNI code and associated MATLAB, python and R scripts to compute various validation metrics are available at `https://github.com/Roy-lab/scMTNI`.

Cell type	Number of edges
C1	202
C2	217
C3	239

Table 1. Statistics of the edges in each cell type for simulated networks.

Gold standards	Number of TFs	Number of targets
ChIP	54	31367
Perturb	179	21019
Perturb+ChIP	47	6109

Table 2. Statistics of the gold standard datasets in mouse ESC from ESCAPE[31] and ENCODE[32] databases and Nishiyama et al[33].

Gold standard	Number of tfs	Number of targets
Hematopoietic stem cells (HSC)	6	9173
CD14_monocytes	1	6523
megakaryocytes	4	8733
erythroid_progenitors	1	7955
R3R4_erythroid_cells	1	8494
megakaryocytes	4	8733
CD34_hematopoietic_stem_cells-derived_proerythroblasts	3	5847
T-cells	3	6189
B-cells	1	7036
GM_B-cells	48	10597
UniBind	56	10621
Cus_ChIP	149	6179
Cus_KO	50	6108
Cus_KO+Cus_ChIP	26	2124
Cus_KO+UniBind	12	2020

Table 3. The statistics of the gold standard datasets in human hematopoietic cell types from UniBind database[42] and Cusanovich et al[43].

References

[1] Constantinos Chronis, Petko Fiziev, Bernadett Papp, Stefan Butz, Giancarlo Bonora, Shan Sabri, Jason Ernst, and Kathrin Plath. Cooperative Binding of Transcription Factors Orchestrates Reprogramming. *Cell*, 168(3):442–459.e20, January 2017.

[2] Zachary D Smith, Camille Sindhu, and Alexander Meissner. Molecular features of cellular reprogramming and development. *Nature Reviews Molecular Cell Biology*, 17(3):139–154, 2016.

[3] Amos Tanay and Aviv Regev. Scaling single-cell genomics from phenomenology to mechanism. *Nature*, 541(7637):331–338, 2017.

[4] Andrew McDavid, Raphael Gottardo, Noah Simon, and Mathias Drton. Graphical Models for Zero-Inflated Single Cell Gene Expression. *The Annals of Applied Statistics*, 13(2):848–873, June 2019. arXiv: 1610.05857.

[5] Thalia E. Chan, Michael P. H. Stumpf, and Ann C. Babtie. Gene Regulatory Network Inference from Single-Cell Data Using Multivariate Information Measures. *Cell Systems*, 5(3):251–267.e3, September 2017.

[6] Hirotaka Matsumoto, Hisanori Kiryu, Chikara Furusawa, Minoru S. H. Ko, Shigeru B. H. Ko, Norio Gouda, Tetsutaro Hayashi, and Itoshi Nikaido. SCODE: an efficient regulatory network inference algorithm from single-cell RNA-Seq during differentiation. *Bioinformatics*, 33(15):2314–2321, August 2017.

[7] Chee Yee Lim, Huange Wang, Steven Woodhouse, Nir Piterman, Lorenz Wernisch, Jasmin Fisher, and Berthold Göttgens. BTR: training asynchronous Boolean models using single-cell expression data. *BMC Bioinformatics*, 17(1):355, September 2016.

[8] Xiaojie Qiu, Arman Rahimzamani, Li Wang, Qi Mao, Timothy Durham, José L. McFaline-Figueroa, Lauren Saunders, Cole Trapnell, and Sreeram Kannan. Towards inferring causal gene regulatory networks from single cell expression Measurements. *bioRxiv*, page 426981, September 2018.

[9] Jukka Intosalmi, Henrik Mannerström, Saara Hiltunen, and Harri Lähdesmäki. SCHiRM: Single Cell Hierarchical Regression Model to detect dependencies in read count data. *bioRxiv*, page 335695, May 2018.

[10] Alicia T. Specht and Jun Li. LEAP: constructing gene co-expression networks for single-cell RNA-sequencing data using pseudotime ordering. *Bioinformatics*, 33(5):764–766, March 2017.

[11] Sara Aibar, Carmen Bravo González-Blas, Thomas Moerman, Vân Anh Huynh-Thu, Hana Imrichova, Gert Hulselmans, Florian Rambow, Jean-Christophe Marine, Pierre Geurts, Jan Aerts, Joost van den Oord, Zeynep Kalender Atak, Jasper Wouters, and Stein Aerts. SCENIC: single-cell regulatory network inference and clustering. *Nature Methods*, 14(11):1083–1086, November 2017.

[12] Rong Zhang, Zhao Ren, and Wei Chen. SILGGM: An extensive R package for efficient statistical inference in large-scale gene networks. *PLOS Computational Biology*, 14(8):e1006369, August 2018.

[13] Andrea Ocone, Laleh Haghverdi, Nikola S. Mueller, and Fabian J. Theis. Reconstructing gene regulatory dynamics from high-dimensional single-cell snapshot data. *Bioinformatics*, 31(12):i89–i96, June 2015.

[14] Chee Yee Lim, Huange Wang, Steven Woodhouse, Nir Piterman, Lorenz Wernisch, Jasmin Fisher, and Berthold Göttgens. Btr: training asynchronous boolean models using single-cell expression data. *BMC bioinformatics*, 17(1):1–18, 2016.

[15] Thalia E Chan, Michael PH Stumpf, and Ann C Babtie. Gene regulatory network inference from single-cell data using multivariate information measures. *Cell systems*, 5(3):251–267, 2017.

[16] Hirotaka Matsumoto, Hisanori Kiryu, Chikara Furusawa, Minoru SH Ko, Shigeru BH Ko, Norio Gouda, Tetsutaro Hayashi, and Itoshi Nikaido. Scode: an efficient regulatory network inference algorithm from single-cell rna-seq during differentiation. *Bioinformatics*, 33(15):2314–2321, 2017.

[17] Aditya Pratapa, Amogh P Jalihal, Jeffrey N Law, Aditya Bharadwaj, and TM Murali. Benchmarking algorithms for gene regulatory network inference from single-cell transcriptomic data. *Nature methods*, 17(2):147–154, 2020.

[18] Matthew Stone, Sunnie Grace McCalla, Alireza Fotuhi Siahpirani, Viswesh Periyasamy, Junha Shin, and Sushmita Roy. Identifying strengths and weaknesses of methods for computational network inference from single cell RNA-seq data. preprint, Bioinformatics, June 2021.

[19] Camden Jansen, Ricardo N Ramirez, Nicole C El-Ali, David Gomez-Cabrero, Jesper Tegner, Matthias Merkenschlager, Ana Conesa, and Ali Mortazavi. Building gene regulatory networks

from scatac-seq and scrna-seq using linked self organizing maps. *PLoS computational biology*, 15(11):e1006555, 2019.

[20] Wanwen Zeng, Xi Chen, Zhana Duren, Yong Wang, Rui Jiang, and Wing Hung Wong. Dc3 is a method for deconvolution and coupled clustering from bulk and single-cell genomics data. *Nature communications*, 10(1):1–11, 2019.

[21] David Heckerman, David Maxwell Chickering, Christopher Meek, Robert Rounthwaite, and Carl Kadie. Dependency networks for inference, collaborative filtering, and data visualization. *Journal of Machine Learning Research*, 1(Oct):49–75, 2000.

[22] Joshua D Welch, Velina Kozareva, Ashley Ferreira, Charles Vanderburg, Carly Martin, and Evan Z Macosko. Single-cell multi-omic integration compares and contrasts features of brain cell identity. *Cell*, 177(7):1873–1887, 2019.

[23] Lennart Kester and Alexander van Oudenaarden. Single-cell transcriptomics meets lineage tracing. *Cell stem cell*, 23(2):166–179, 2018.

[24] Christopher Koch, Jay Konieczka, Toni Delorey, Ana Lyons, Amanda Socha, Kathleen Davis, Sara A Knaack, Dawn Thompson, Erin K O'Shea, Aviv Regev, et al. Inference and evolutionary analysis of genome-scale regulatory networks in large phylogenies. *Cell systems*, 4(5):543–558, 2017.

[25] Emma Pierson, Daphne Koller, Alexis Battle, Sara Mostafavi, GTEx Consortium, et al. Sharing and specificity of co-expression networks across 35 human tissues. *PLoS Comput Biol*, 11(5):e1004220, 2015.

[26] Vladimir Jojic, Tal Shay, Katelyn Sylvia, Or Zuk, Xin Sun, Joonsoo Kang, Aviv Regev, and Daphne Koller. Identification of transcriptional regulators in the mouse immune system. *Nature immunology*, 14(6):633–643, 2013.

[27] Dayanne M Castro, Nicholas R De Veaux, Emily R Miraldi, and Richard Bonneau. Multi-study inference of regulatory networks for more accurate models of gene regulation. *PLoS computational biology*, 15(1):e1006591, 2019.

[28] Robert Tibshirani. Regression shrinkage and selection via the lasso. *Journal of the Royal Statistical Society: Series B (Methodological)*, 58(1):267–288, 1996.

[29] Sara Aibar, Carmen Bravo González-Blas, Thomas Moerman, Hana Imrichova, Gert Hulselmans, Florian Rambow, Jean-Christophe Marine, Pierre Geurts, Jan Aerts, Joost van den Oord, et al. Scenic: single-cell regulatory network inference and clustering. *Nature methods*, 14(11):1083–1086, 2017.

[30] Rupa Sridharan and Kathrin Plath. Illuminating the black box of reprogramming. *Cell Stem Cell*, 2(4):295–297, April 2008.

[31] Huilei Xu, Caroline Baroukh, Ruth Dannenfelser, Edward Y Chen, Christopher M Tan, Yan Kou, Yujin E Kim, Ihor R Lemischka, and Avi Ma'ayan. Escape: database for integrating high-content published data collected from human and mouse embryonic stem cells. *Database (Oxford)*, 2013:bat045, 2013.

[32] ENCODE Project Consortium. An integrated encyclopedia of DNA elements in the human genome. *Nature*, 489(7414):57–74, 2012.

[33] Akira Nishiyama, Li Xin, Alexei A Sharov, Marshall Thomas, Gregory Mowrer, Emily Meyers, Yulan Piao, Samir Mehta, Sarah Yee, Yuhki Nakatake, et al. Uncovering early response of gene regulatory networks in escs by systematic induction of transcription factors. *Cell stem cell*, 5(4):420–433, 2009.

[34] Pei-Shan Hou, Ching-Yu Chuang, Cheng-Fu Kao, Shen-Ju Chou, Lee Stone, Hong-Nerng Ho, Chung-Liang Chien, and Hung-Chih Kuo. LHX2 regulates the neural differentiation of human embryonic stem cells via transcriptional modulation of PAX6 and CER1. *Nucleic Acids Research*, 41(16):7753–7770, September 2013.

[35] Aileen M. Smith, Fernando J. Calero-Nieto, Judith Schütte, Sarah Kinston, Richard T. Timms, Nicola K. Wilson, Rebecca L. Hannah, Josette-Renee Landry, and Berthold Göttgens. Integration of Elf-4 into stem/progenitor and erythroid regulatory networks through locus-wide chromatin studies coupled with in vivo functional validation. *Molecular and Cellular Biology*, 32(4):763–773, February 2012.

[36] Shaoke Lou, Tianxiao Li, Xiangmeng Kong, Jing Zhang, Jason Liu, Donghoon Lee, and Mark Gerstein. Topicnet: a framework for measuring transcriptional regulatory network change. *Bioinformatics*, 36(Supplement_1):i474–i481, 2020.

[37] L1 Yang, Y Han, F Saurez Saiz, and MD Minden. A tumor suppressor and oncogene: the wt1 story. *Leukemia*, 21(5):868–876, 2007.

[38] Yan Liu, Ruben Hoya-Arias, and Stephen D Nimer. The role of p53 in limiting somatic cell reprogramming. *Cell Research*, 19(11):1227–1228, 2009.

[39] Yang Zhao, Xiaolei Yin, Han Qin, Fangfang Zhu, Haisong Liu, Weifeng Yang, Qiang Zhang, Chengang Xiang, Pingping Hou, Zhihua Song, et al. Two supporting factors greatly improve the efficiency of human ipsc generation. *Cell stem cell*, 3(5):475–479, 2008.

[40] Kazutoshi Takahashi and Shinya Yamanaka. Induction of pluripotent stem cells from mouse embryonic and adult fibroblast cultures by defined factors. *cell*, 126(4):663–676, 2006.

[41] Jason D Buenrostro, M Ryan Corces, Caleb A Lareau, Beijing Wu, Alicia N Schep, Martin J Aryee, Ravindra Majeti, Howard Y Chang, and William J Greenleaf. Integrated single-cell analysis maps the continuous regulatory landscape of human hematopoietic differentiation. *Cell*, 173(6):1535–1548, 2018.

[42] Rafael Riudavets Puig, Paul Boddie, Aziz Khan, Jaime Abraham Castro-Mondragon, and Anthony Mathelier. Unibind: maps of high-confidence direct tf-dna interactions across nine species. *bioRxiv*, pages 2020–11, 2021.

[43] Darren A. Cusanovich, Bryan Pavlovic, Jonathan K. Pritchard, and Yoav Gilad. The functional consequences of variation in transcription factor binding. *PLoS Genet*, 10(3):e1004226+, March 2014.

[44] Jasjeet Bhullar and Vincent E Sollars. Ybx1 expression and function in early hematopoiesis and leukemic cells. *Immunogenetics*, 63(6):337–350, 2011.

[45] Byunghee Koh, Matthew M. Hufford, Duy Pham, Matthew R. Olson, Tong Wu, Rukhsana Jabeen, Xin Sun, and Mark H. Kaplan. The ETS Family Transcription Factors Etv5 and PU.1 Function in Parallel To Promote Th9 Cell Development. *Journal of Immunology (Baltimore, Md.: 1950)*, 197(6):2465–2472, September 2016.

[46] Laura G. Schuettpelz, Priya K. Gopalan, Felipe O. Giuste, Molly P. Romine, Ronald van Os, and Daniel C. Link. Kruppel-like factor 7 overexpression suppresses hematopoietic stem and progenitor cell function. *Blood*, 120(15):2981–2989, October 2012.

[47] R. C. Briggs, W. Y. Kao, L. L. Dworkin, J. A. Briggs, E. N. Dessypris, and J. Clark. Regulation and specificity of MNDA expression in monocytes, macrophages, and leukemia/B lymphoma cell lines. *Journal of Cellular Biochemistry*, 56(4):559–567, December 1994.

[48] Shuyang Yu, Kairong Cui, Raja Jothi, Dong-Mei Zhao, Xuefang Jing, Keji Zhao, and Hai-Hui Xue. Gabp controls a critical transcription regulatory module that is essential for maintenance and differentiation of hematopoietic stem/progenitor cells. *Blood, The Journal of the American Society of Hematology*, 117(7):2166–2178, 2011.

[49] H Daniel Lacorazza, Takeshi Yamada, Yan Liu, Yasuhiko Miyata, Mariela Sivina, Juliana Nunes, and Stephen D Nimer. The transcription factor mef/elf4 regulates the quiescence of primitive hematopoietic cells. *Cancer cell*, 9(3):175–187, 2006.

[50] Christina Alidousty, Thomas Rauen, Lydia Hanssen, Qiang Wang, Setareh Alampour-Rajabi, Peter R Mertens, Jürgen Bernhagen, Jürgen Floege, Tammo Ostendorf, and Ute Raffetseder. Calcineurin-mediated yb-1 dephosphorylation regulates ccl5 expression during monocyte differentiation. *Journal of Biological Chemistry*, 289(31):21401–21412, 2014.

[51] Zenobio Viana de Barros, Stefano Bruscoli, Sara Flamini, Tiziana Frammartino, Andrea Gagliardi, Graziella Migliorati, Carlo Riccardi, and Oxana Bereshchenko. 3142–glucocorticoid-induced leucine zipper (gilz) intrinsically regulates hematopoietic stem cell function. *Experimental Hematology*, 88:S82, 2020.

[52] M Dolores Delgado and Javier León. Myc roles in hematopoiesis and leukemia. *Genes & cancer*, 1(6):605–616, 2010.

[53] Louis C Doré and John D Crispino. Transcription factor networks in erythroid cell and megakaryocyte development. *Blood, The Journal of the American Society of Hematology*, 118(2):231–239, 2011.

[54] Miroslawa Siatecka and James J Bieker. The multifunctional role of eklf/klf1 during erythropoiesis. *Blood, The Journal of the American Society of Hematology*, 118(8):2044–2054, 2011.

[55] Cuiping Zhang, Yvonne N. Fondufe-Mittendorf, Chi Wang, Jin Chen, Qiang Cheng, Daohong Zhou, Yi Zheng, Hartmut Geiger, and Ying Liang. Latexin regulation by HMGB2 is required for hematopoietic stem cell maintenance. *Haematologica*, 105(3):573–584, March 2020.

[56] Emily R. Miraldi, Maria Pokrovskii, Aaron Waters, Dayanne M. Castro, Nick De Veaux, Jason Hall, June-Yong Lee, Maria Ciofani, Aviv Madar, Nick Carriero, and et al. Leveraging chromatin accessibility for transcriptional regulatory network inference in t helper 17 cells. *Genome Research*, page gr.238253.118, Jan 2019.

[57] Sushmita Roy, Stephen Lagree, Zhonggang Hou, James A. Thomson, Ron Stewart, and Audrey P. Gasch. Integrated module and Gene-Specific regulatory inference implicates upstream signaling networks. *PLoS Comput. Biol.*, 9(10):e1003252+, October 2013.

[58] Jean Fan, Neeraj Salathia, Rui Liu, Gwendolyn E Kaeser, Yun C Yung, Joseph L Herman, Fiona Kaper, Jian-Bing Fan, Kun Zhang, Jerold Chun, et al. Characterizing transcriptional heterogeneity through pathway and gene set overdispersion analysis. *Nature methods*, 13(3):241–244, 2016.

[59] Yong Zhang, Tao Liu, Clifford A Meyer, Jérôme Eeckhoute, David S Johnson, Bradley E Bernstein, Chad Nusbaum, Richard M Myers, Myles Brown, Wei Li, et al. Model-based analysis of chip-seq (macs). *Genome biology*, 9(9):1–9, 2008.

[60] Matthew T. Weirauch, Ally Yang, Mihai Albu, Atina G. Cote, Alejandro Montenegro-Montero, Philipp Drewe, Hamed S. Najafabadi, Samuel A. Lambert, Ishminder Mann, Kate Cook, Hong Zheng, Alejandra Goity, Harm van Bakel, Jean-Claude Lozano, Mary Galli, Mathew G. Lewsey, Eryong Huang, Tuhin Mukherjee, Xiaoting Chen, John S. Reece-Hoyes, Sridhar Govindarajan, Gad Shaulsky, Albertha J M. Walhout, François-Yves Bouget, Gunnar Ratsch, Luis F. Larrondo, Joseph R. Ecker, and Timothy R. Hughes. Determination and inference of eukaryotic transcription factor sequence specificity. *Cell*, 158(6):1431–1443, Sep 2014.

[61] Richard I Sherwood, Tatsunori Hashimoto, Charles W O'Donnell, Sophia Lewis, Amira A Barkal, John Peter van Hoff, Vivek Karun, Tommi Jaakkola, and David K Gifford. Discovery of directional and nondirectional pioneer transcription factors by modeling dnase profile magnitude and shape. *Nature biotechnology*, 32:171–178, February 2014.

[62] Khoa A Tran, Stefan J Pietrzak, Nur Zafirah Zaidan, Alireza Fotuhi Siahpirani, Sunnie Grace McCalla, Amber S Zhou, Gopal Iyer, Sushmita Roy, and Rupa Sridharan. Defining reprogramming checkpoints from single-cell analyses of induced pluripotency. *Cell reports*, 27(6):1726–1741, 2019.

[63] Thomas Moerman, Sara Aibar Santos, Carmen Bravo González-Blas, Jaak Simm, Yves Moreau,

961 Jan Aerts, and Stein Aerts. Grnboost2 and arboreto: efficient and scalable inference of gene regu-
962 latory networks. *Bioinformatics*, 35(12):2159–2161, 2019.

963 [64] Jesse Davis and Mark Goadrich. The relationship between precision-recall and roc curves. In
964 *Proceedings of the 23rd international conference on Machine learning*, pages 233–240, 2006.

965 [65] Michael Ashburner, Catherine A Ball, Judith A Blake, David Botstein, Heather Butler, J Michael
966 Cherry, Allan P Davis, Kara Dolinski, Selina S Dwight, Janan T Eppig, et al. Gene ontology: tool
967 for the unification of biology. *Nature genetics*, 25(1):25–29, 2000.

968 [66] The ENCODE Project Consortium. Identification and analysis of functional elements in 1% of the
969 human genome by the ENCODE pilot project. *Nature*, 447(7146):799–816, 2007.

Acknowledgements

We thank the Center for High Throughput Computing at University of Wisconsin-Madison for computational resources. This work is supported by the National Institutes of Health NIGMS grant 1R01GM117339.

Author contributions

S.Z. and S.R. designed the scMTNI algorithm and experiments. S.Z. implemented the code and performed most of the experiments. S.P. contributed towards creation of the gold standards and evaluating selected algorithms. S.P. and R.S. generated the scATAC-seq data for the reprogramming experiments. All authors contributed towards writing the manuscript.

Competing Interests

The authors declare no competing interests.

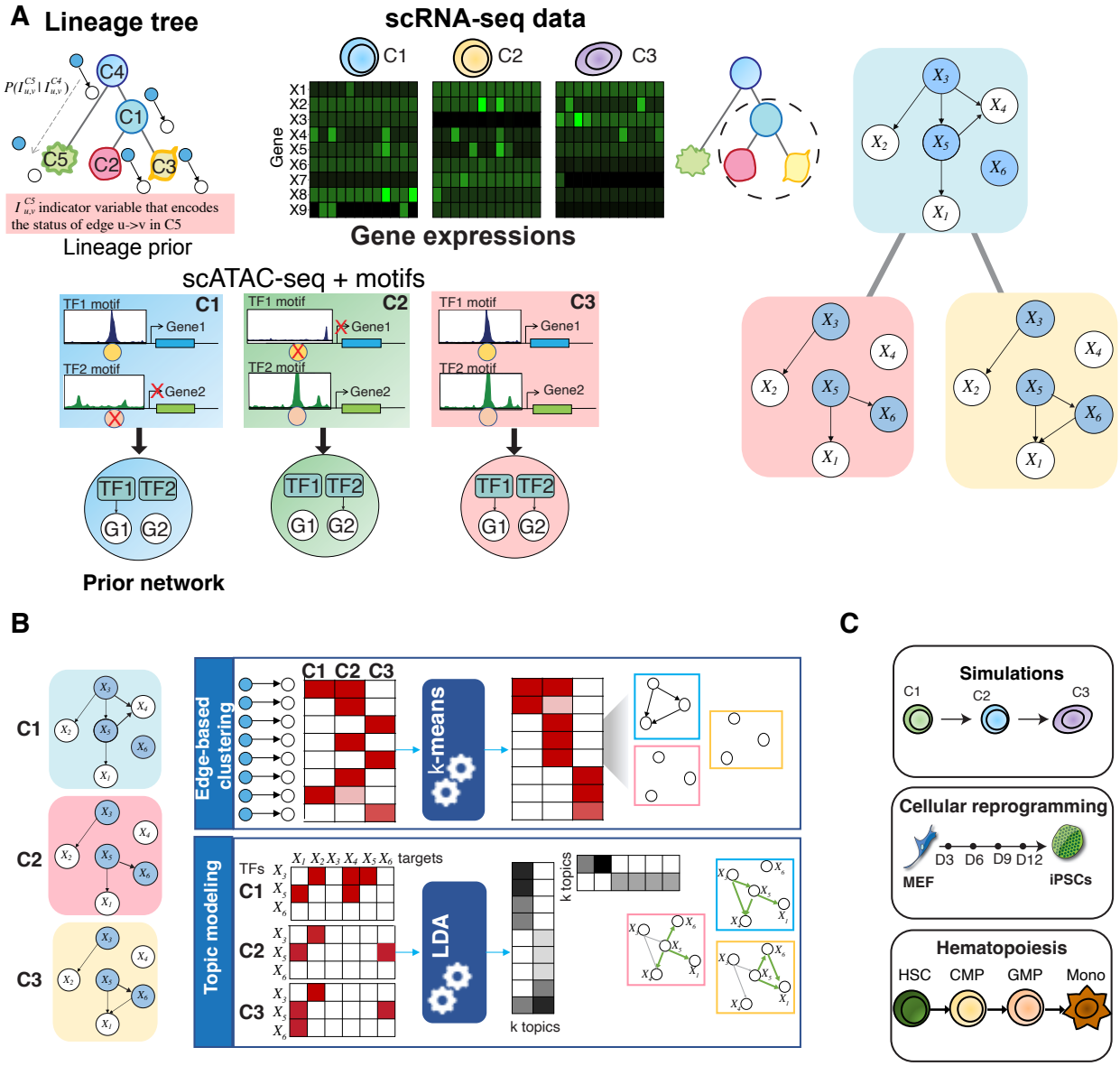

Figure 1. An overview of the scMTNI framework. **A.** scMTNI takes as input a cell lineage tree and cell type-specific scRNA-seq data and cell type-specific prior networks derived from single cell ATAC-seq datasets. If scATAC-seq data is not available, the same prior network can be used for all cell types. The output of scMTNI is a set of cell type-specific gene regulatory networks for each cell type on the cell lineage tree. **B.** The output networks of scMTNI are analyzed using two dynamic network analysis methods: edge-based k-means clustering and Latent Dirichlet Allocation (LDA) based topic models to identify key regulators and subnetworks associated with a particular cell cluster or a set of clusters on a branch. **C.** Datasets used with scMTNI. The simulation data comprised a linear trajectory of three cell types, while the two real datasets came from a reprogramming time-series process and immunophenotypic cell types identified during human hematopoietic differentiation.

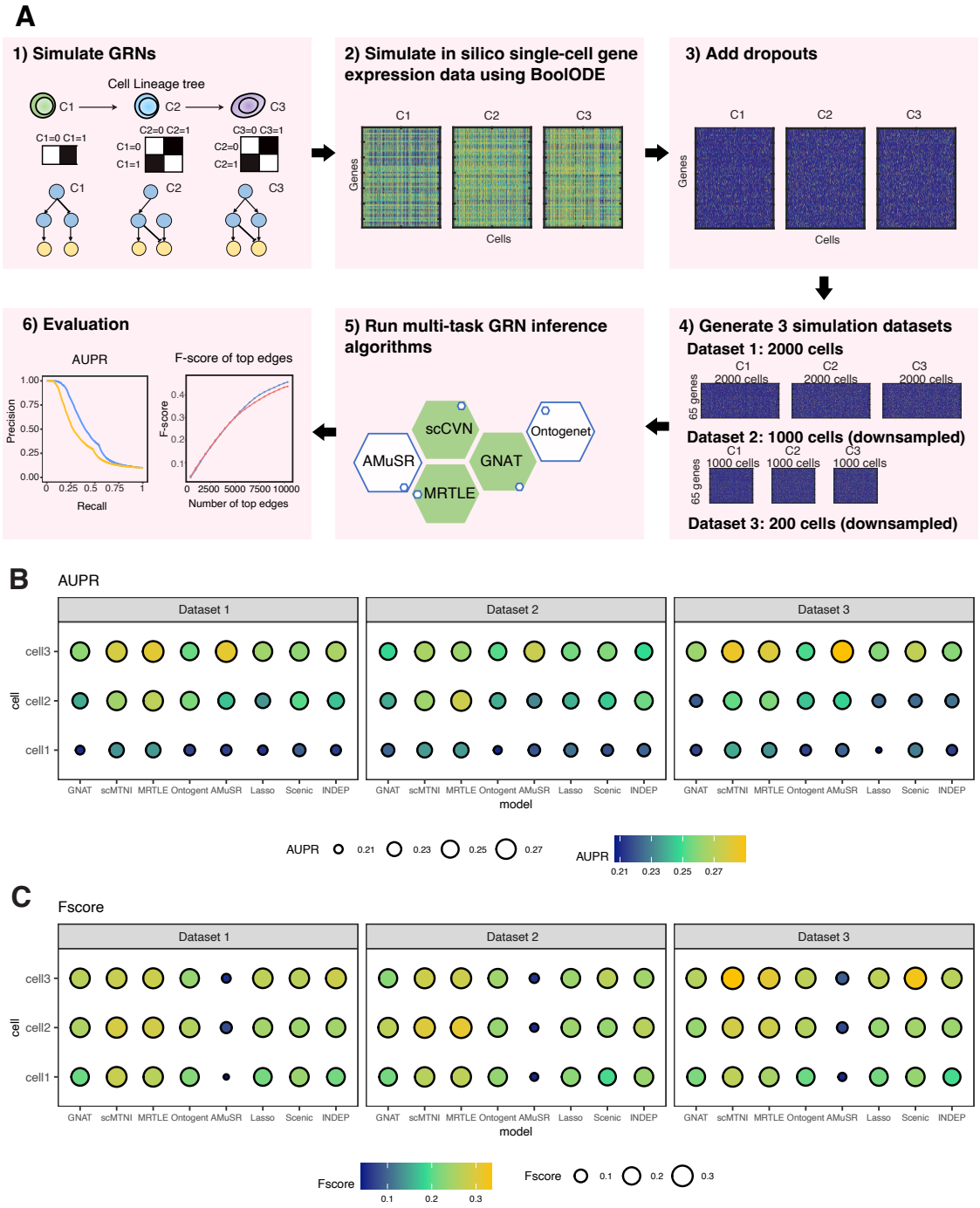

Figure 2. Benchmarking algorithms on simulated data. **A.** Simulation framework for scMTNI. We first simulate GRNs for cell types across a cell lineage tree. Next, we generate *in silico* single-cell gene expression data for each cell type using BoolODE using the simulated GRNs and add 80% zeros in the simulation data. Then, we apply five multi-task learning algorithms for GRN inference to the simulated datasets and predict networks in stability selection framework. We compare the performance of these algorithms based on area under precision and recall curve (AUPR) and F-score of top edges. **B.** AUPR comparing inferred networks to ground truth networks of simulated datasets 1, 2, 3. **C.** F-score comparing top K edges in the inferred networks to those in the ground truth networks of simulated datasets 1, 2, 3. The brighter and larger the circle the better the performance of the algorithm.

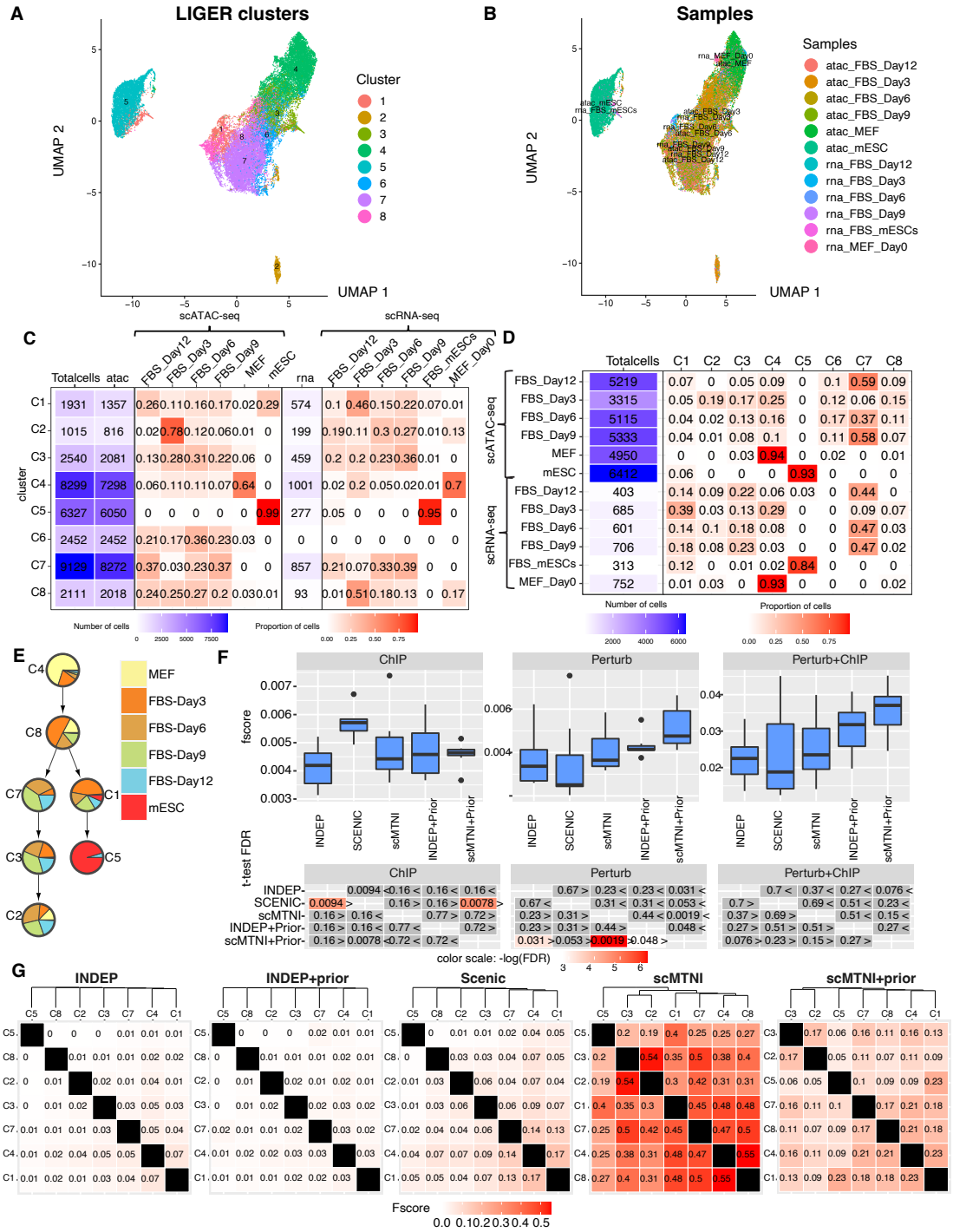

Figure 3. Inference of cell-type specific networks of mouse reprogramming data. **A.** UMAP of LIGER cell clusters on the scATAC-seq data and scRNA-seq data. **B.** UMAP depicting the sample labels of the scATAC-seq and scRNA-seq data. **C.** The distribution of LIGER clusters in each sample. **D.** The distribution of samples for each LIGER cluster. **E.** Inferred lineage structure for scMTNI linking the 7 cell clusters with scRNA-seq measurements. **F.** F-score of top 1k edges in predicted networks of scMTNI, scMTNI+prior, INDEP, INDEP+prior, and SCENIC compared to three gold standard datasets: ChIP, Perturb and Perturb+ChIP. The top boxplots show the F-scores, while the bottom heatmaps show FDR corrected T-test comparing the F-scores of the row algorithm to that of the column algorithm. A FDR$<$0.05 was considered significantly better. The sign $<$ or $>$ specifies whether the row algorithm's F-scores were worse or better than the column algorithm's F-scores. The color scale is specified for $-log(FDR)$, with the red color proportional to significance. **G.** Pairwise similarity of networks from each cell cluster using F-score on the top 4k edges. Rows and columns are ordered based on the dendrogram created using the F-score similarity.

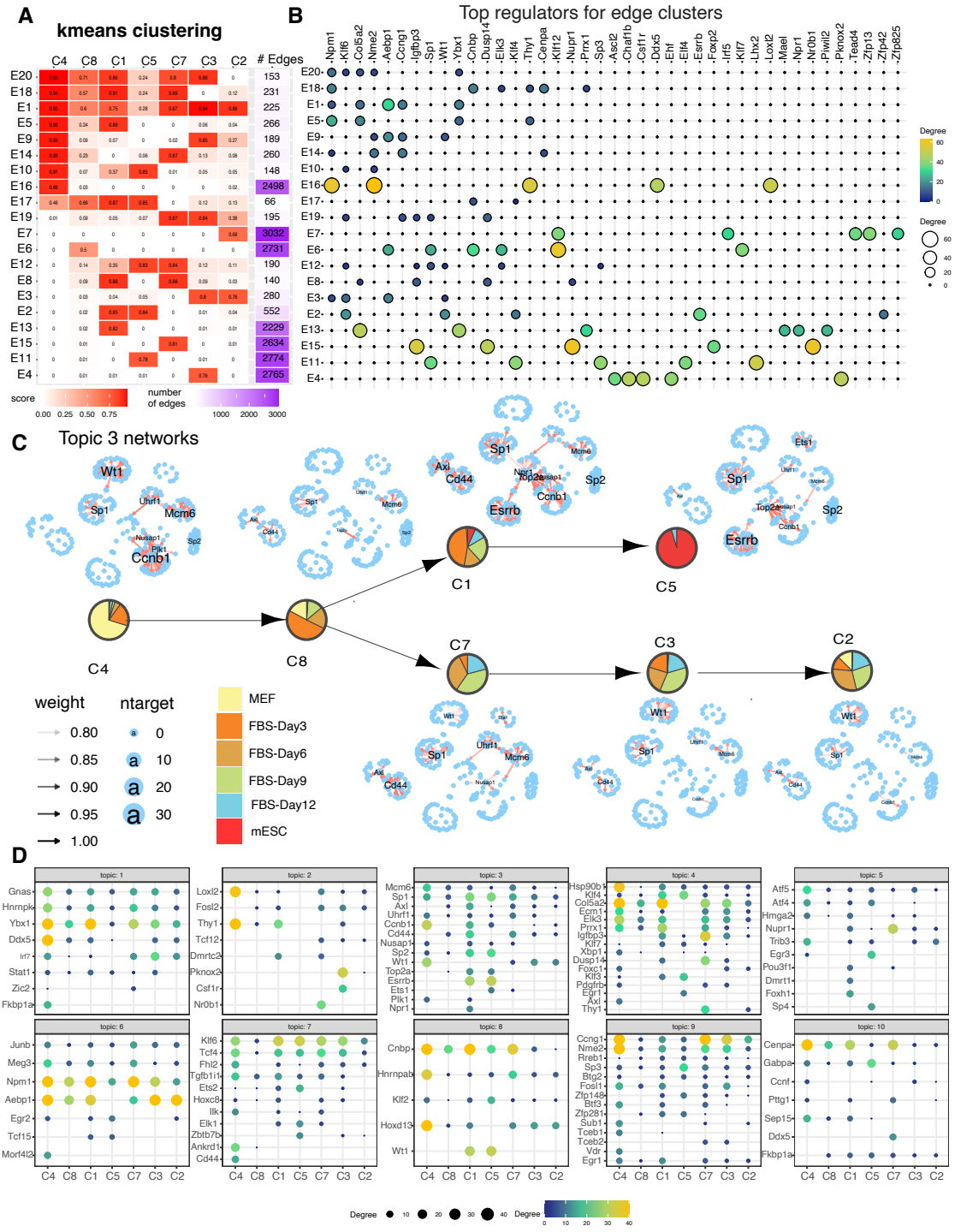

Figure 4. Network dynamics analysis of GRNs from cellular reprogramming. **A.** Kmeans clustering analysis of inferred networks. Shown are the mean profiles of edge confidence of 20 edge clusters. Each row corresponds to an edge cluster and each column corresponds to a cell cluster. The red intensity corresponds to the average confidence of edges in that cluster. Shown also are the number of edges in the edge cluster. **B.** Top regulators for each edge cluster. Shown are only regulators that have at least 10 targets in any edge cluster. The size and brightness of the circle is proportional to the number of targets. **C.** LDA topic 3 networks along the cell lineage. The layout of each network is the same, edges present in a particular cell cluster are shown in red. Labeled nodes correspond to regulators with the largest number of connections **D.** Cell cluster-specific regulators for each topic. The brighter and larger the circle, the greater are the number of targets for the regulator.

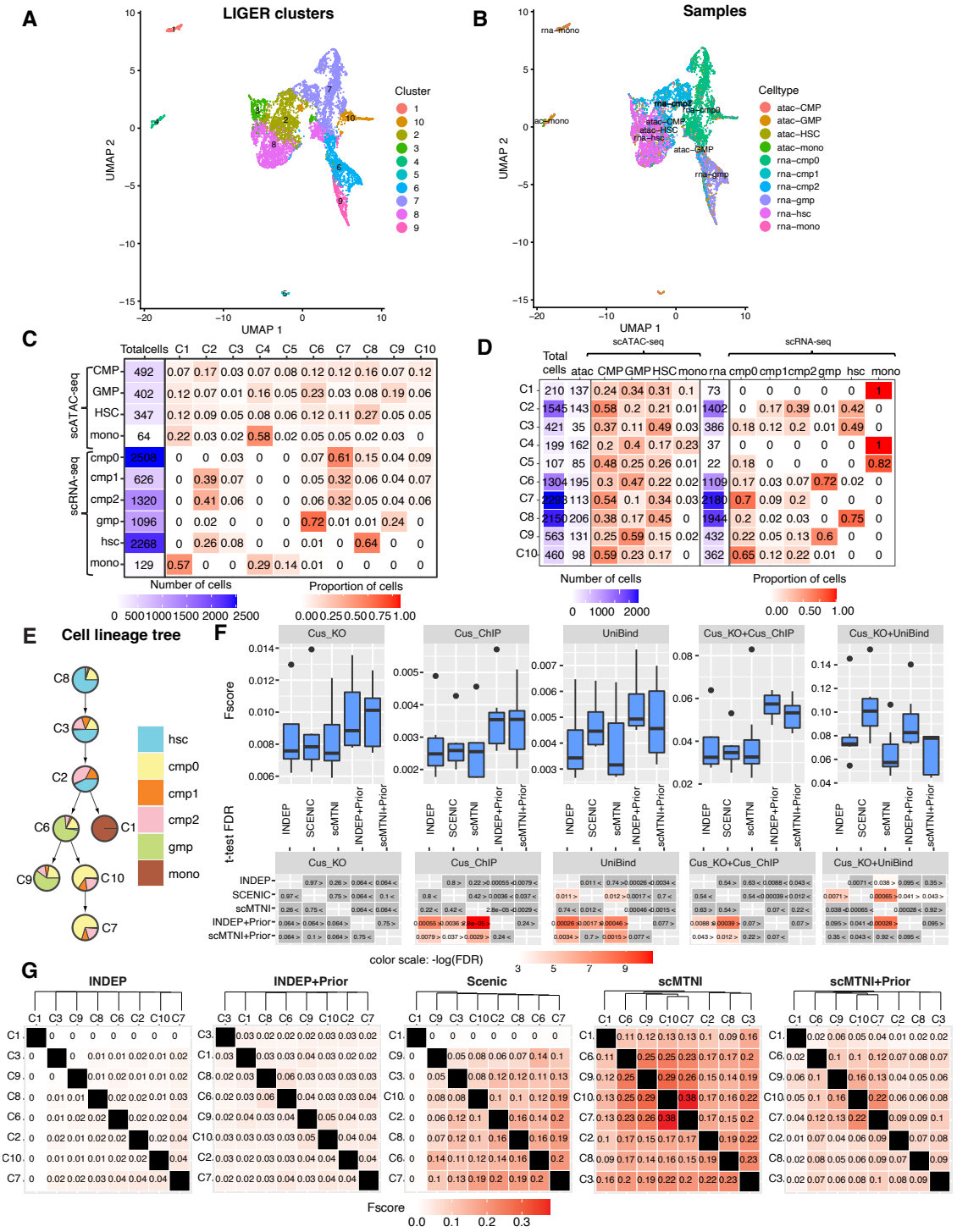

Figure 5. scMTNI networks on human hematopoietic differentiation data. **A.** UMAP of LIGER cell clusters of the scATAC-seq and scRNA-seq data. **B.** UMAP depicting the original cell types (samples) with scATAC-seq and scRNA-seq data. **C.** The distribution of samples for each LIGER cluster. **D.** The distribution of cell clusters for each sample. **E.** Inferred lineage structure linking the eight cell clusters with scRNA-seq and scATAC-seq data. **F.** Boxplots showing F-score of top 1k edges in predicted networks from scMTNI, scMTNI+prior, INDEP, INDEP+prior, and SCENIC compared to gold standard datasets (top). FDR-corrected T-test to compare the F-score of the row algorithm to the F-score of the column algorithm (bottom). A FDR$<$0.05 was considered significantly better. The sign $<$ or $>$ specifies whether the row algorithm's F-scores were worse or better than the column algorithm's F-scores. The color scale is specified for $-log(FDR)$, with the red color proportional to significance. **G.** Pairwise similarity of networks from each cell cluster using F-score on the top 5k edges which corresponds to a confidence of $\sim$0.8. Rows and columns ordered by hierarchical clustering using F-score as the similarity measure.

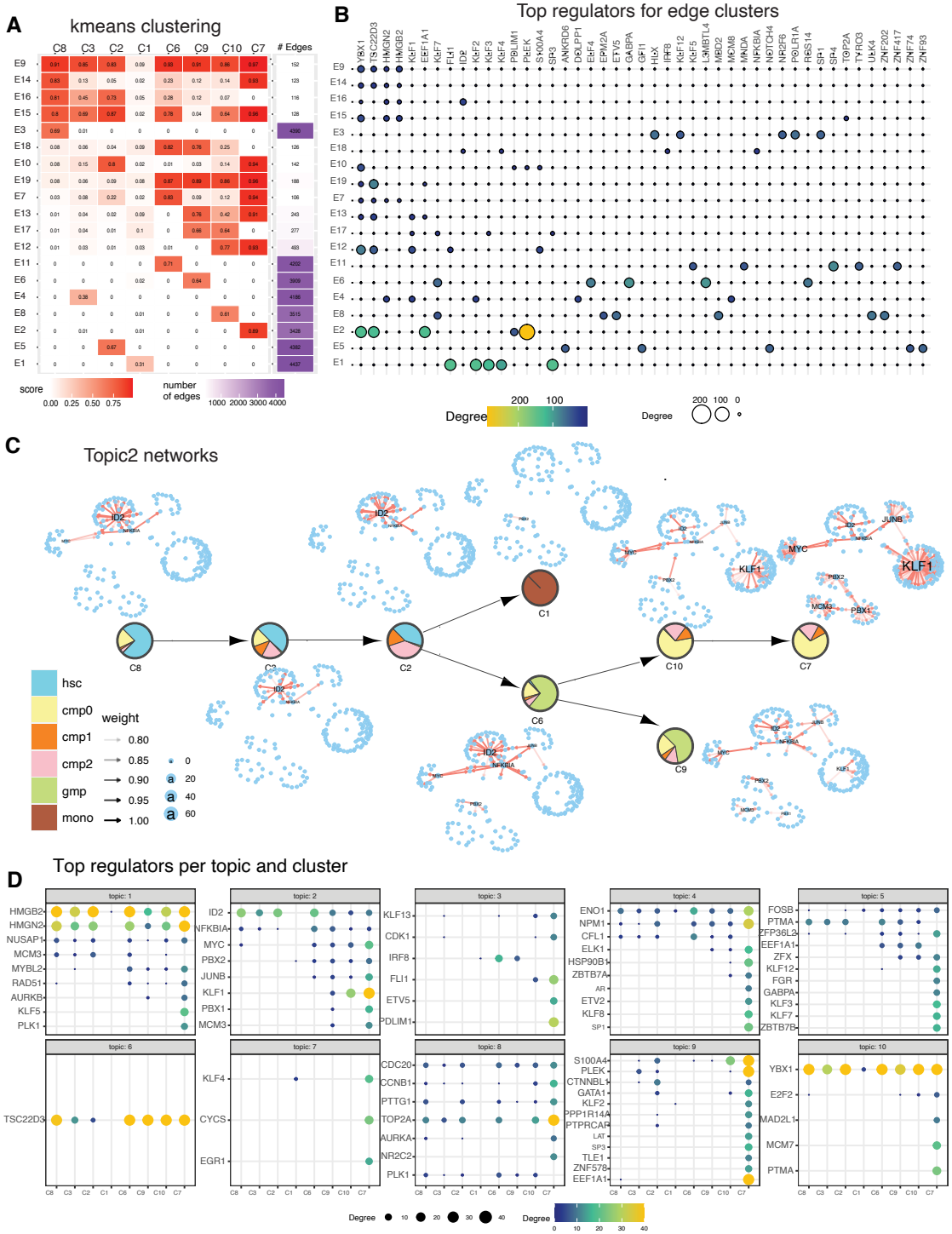

Figure 6. Network rewiring during hematopoietic differentiation. **A.** Kmeans-based edge clusters of the top 5k edges (rows) across 8 cell clusters (columns). The edge confidence matrix was clustered into 19 clusters to identify common and divergent networks. The red intensity corresponds to the average confidence of edges in that cluster. Shown also are the number of edges in the edge cluster. **B.** Top regulators of each edge cluster. Shown are only regulators with at least 10 targets in a given edge cluster. The size and brightness of the circle is proportional to the number of targets. **C.** Topic-specific networks across each cell cluster for topic 4. The layout of each network is the same, edges present in a particular cell cluster are shown in red. Labeled nodes correspond to regulators with the largest number of connections. **D.** Regulators associated with each cell cluster's network in each topic.The brighter and larger the circle, the greater are the number of targets for the regulator.